Universitat Autònoma de Barcelona

ELUCIDATING REACTION MECHANISMS FOR METAL-CATALYZED OXIDATIONS

Laia Vilella Arribas

ADVERTIMENT. L'accés als continguts d'aquesta tesi queda condicionat a l'acceptació de les condicions d'ús establertes per la següent llicència Creative Commons: http://cat.creativecommons.org/?page_id=184

ADVERTENCIA. El acceso a los contenidos de esta tesis queda condicionado a la aceptación de las condiciones de uso establecidas por la siguiente licencia Creative Commons: http://es.creativecommons.org/blog/licencias/

WARNING. The access to the contents of this doctoral thesis it is limited to the acceptance of the use conditions set by the following Creative Commons license: https://creativecommons.org/licenses/?lang=en

Universitat Autònoma de Barcelona

ELUCIDATING REACTION MECHANISMS FOR METAL-CATALYZED OXIDATIONS

Laia Vilella Arribas

Ph.D. Thesis
Chemistry

Supervisors:

David Balcells Badia
Agustí Lledós Falcó

Departament de Química
Facultat de Ciències

2015

Universitat Autònoma de Barcelona
Departament de Química
Unitat de Química Física

Memòria presentada per aspirar al Grau de Doctor per Laia Vilella Arribas

Laia Vilella Arribas

Vist i plau,

David Balcells Badia   Agustí Lledós Falcó

Bellaterra, 19 d'octubre de 2015

Acknowledgments

Unofficial Acknowledgments

Abans de començar a parlar pròpiament de ciència, volia dedicar aquesta tesi doctoral a totes aquelles persones que han estat al meu costat i que m'han donat suport durant tot aquest temps.

Primerament, voldria donar les gràcies als meus directors de tesis Agustí Lledós i David Balcells. Agustí, gràcies per donar-me l'oportunitat de formar part del grup Transmet, i per la teva perseverança i motivació per la recerca; i David, per haver-me introduït en aquest món i ensenyar-me tot el que sé de catàlisis homogènia. En aquest context he d'anomenar també a la professora Núria López per haver-me acollit uns mesos a l'ICIQ i iniciat en l'estudi de sistemes catalítics heterogenis, i a la doctora Aleksandra Vojvodic de la Universitat de Stanford per fer-me recuperar la il·lusió per la investigació.

Estic especialment agraïda a tots els companys de despatx, tot ells grans persones i científics, el quals ja són pràcticament tots doctors i es troben escampats arreu del món. No oblidaré mai els moments que hem passat junts, tant immersos en l'ambient de treball com evadits de ciència. No vull deixar de mencionar a la resta de gent del departament de química física de la UAB, als companys de màster, així com tampoc a tota la gent que he tingut la oportunitat de conèixer durant les estades realitzades a l'ICIQ i a la Universitat de Stanford.

He de reconèixer que no m'hauria imaginat mai arribar fins aquí i realment qui ho ha fet possible han estat els meus pares, avis i sobretot el Max. Gràcies pel vostre recolzament i per ajudar-me a seguir endavant.

Official Acknowledgments

I would like to thank Ministerio de Educación, Cultura y Deporte (Government of Spain) for the predoctoral FPU fellowship that made possible the present PhD thesis and the travel scholarship that allowed a temporary stay in the research group of Prof. Jens K. Nørskov (University of Stanford) under the supervision of Dr. Felix Studt.

Prof. Pedro J. Pérez, Dr. M. Mar Díaz Requejo and Dr. Ana Conde from the CIQSO-Centro de Investigación en Química Sostenible (Universidad de Huelva) are also acknowledged for their collaboration in some of studies presented in this thesis.

Als meus pares, avis i al Max

Contents

CHAPTER 1: Introduction 1

1.1. Basic Concepts 3
  1.1.1. Reaction Mechanism 3
  1.1.2. Catalysis 4
    1.1.2.1. Homogeneous Catalysis 8
    1.1.2.2. Heterogeneous Catalysis 9
    1.1.2.3. Homogeneous *vs.* Heterogeneous Catalysis 10

1.2. Oxidation Reactions 12
  1.2.1. Water Oxidation 12
    1.2.1.1. Reaction Mechanisms 15
  1.2.2. C=C Oxidation 16
    1.2.2.1. Reaction Mechanisms 17
  1.2.3. C−H Oxidation 19
    1.2.3.1. Reaction Mechanisms 21
  1.2.4. C−C Oxidation to C=C 24
    1.2.4.1. Reaction Mechanisms 25

CHAPTER 2: Computational Details 27

2.1. Quantum Mechanics 29

2.2. Density Functional Theory 31
  2.2.1. Exchange-Correlation Energy 32
  2.2.2. Description of Open-shell Systems 35

2.3. Scope of Application 36
  2.3.1. Exchange-Correlation Functionals Employed 36
  2.3.2. Basis Sets 37
    2.3.2.1. Orbital-like Functions 37
    2.3.2.2. Plane Wave Functions 39

2.3.3. Potential Energy Surface 40
  2.3.3.1. Minimum Energy Crossing Points 42
2.3.4. Solvation Models 43
2.3.5. Gibbs Energies in Solution 44

CHAPTER 3: Objectives 47

CHAPTER 4: Bernhard's Water Oxidation Catalyst 51

4.1. Introduction 53
  4.1.1. Bernhard's Catalyst 54
4.2. Computational Details 57
4.3. Results 58
  4.3.1. O−O Bond Formation Mechanism 58
  4.3.2. Electronic Structure Analysis 64
4.4. Discussion and Conclusions 67

CHAPTER 5: Comparing Model Ir-based Water Oxidation Catalysts 69

5.1. Introduction 71
5.2. Computational Details 72
5.3. Results 75
  5.3.1. Stability of the Ir Hybrid Catalyst 75
  5.3.2. Catalytic Active Species 76
  5.3.2.1. Active Species for the $IrO_2(110)$ Surface Catalyst 77
  5.3.2.2. Active Species for the Dimeric Ir Catalyst 78
  5.3.2.3. Active Species for the Ir Hybrid Catalyst 81
  5.3.3. Reaction Mechanisms 83
    5.3.3.1. Water oxidation with $IrO_2(110)$ Surface Catalyst 84
    5.3.3.2. Water oxidation with the Dimeric Ir Catalyst 86

5.3.3.3. Water oxidation with the Ir-Hybrid Catalyst 88
5.3.4. Bader Charge Analysis 90
5.4. Discussion and Conclusions 91
Appendix 93

CHAPTER 6: Rhodium- and Iridium-Mediated Alkene Oxidation with O_2 103

6.1. Introduction 105
6.2. Computational Details 106
6.3. Results 108
6.3.1. Reaction Mechanisms 108
6.3.1.1. Oxidation with the [Rh(PhN_3Ph)(cod)] complex 109
6.3.1.2. Spin Density Analysis 115
6.3.1.3. Oxidation with the [Ir(PhN=C(NMe_2)NPh)(cod)] complex 116
6.3.1.4. Effect of the Transition Metal 124
6.3.2. Factors Governing Alkene Oxidation 126
6.4. Discussion and Conclusions 130
Appendix 132

CHAPTER 7: Copper-Catalyzed Oxidation of Aromatic C–H Bonds 135

7.1. Introduction 137
7.2. Experimental Results 138
7.3. Computational Details 145
7.4. Theoretical Results 146
7.4.1. Catalytic Active Species 146
7.4.2. Reaction Mechanisms 148
7.4.2.1. Electrophilic Aromatic Substitution (S_EAr) on Benzene 148

7.4.2.2. Electrophilic Aromatic Substitution ($\mathrm{S_EAr}$) on Substituted Benzenes 152
7.4.2.3. Rebound Mechanism on Benzene 154
7.4.2.4. Rebound Mechanism on Substituted Benzenes 157
7.4.2.5. Benzene Oxidation by Superoxo and Hydroperoxo Species 159

7.5. Discussion and Conclusions 162

Appendix 164

CHAPTER 8: Copper-Catalyzed Hydroxylation & Dehydrogenation of Alkanes 167

8.1. Introduction 169

8.2. Experimental Results 170

8.3. Computational Details 175

8.4. Theoretical Results 176
8.4.1. Reaction Mechanisms 176
8.4.1.1. Hydroxylation and Dehydrogenation of Cyclohexane with the Cu-Oxo Species 176
8.4.1.2. Hydroxylation and Dehydrogenation of Cyclohexane with Cu-Superoxo and Hydroperoxo Species 182

8.5. Discussion and Conclusions 183

CHAPTER 9: General Conclusions 185

Bibliography 189

"There are no more than two rules for writing: having something to say, and saying it."

Oscar Wilde

1

Introduction

This first chapter is devoted to give an overview of the main topics covered in this Ph.D. thesis. First, some basic concepts such as reaction mechanism and catalysis are introduced. Next, a more detailed description of homogeneous and heterogeneous catalysis, including their respective strengths and weaknesses is provided. Finally, the oxidation reactions investigated in this thesis and their most important industrial applications are presented. For these reactions, the most relevant mechanistic studies reported in the literature are briefly reviewed.

1.1. Basic Concepts

1.1.1. Reaction Mechanism

In a chemical reaction one or more species, i.e. reactants, are transformed leading to a different set of compounds, i.e. products. The description of what occurs at each stage of the overall chemical process is known as *reaction mechanism*. A good knowledge of reaction mechanisms is crucial as it can provide detailed guidance to further improve chemical processes. Hence, by understanding the most relevant features of a given reaction, new strategies to achieve higher rates, yields and/or selectivities can be developed. Unfortunately, the many steps typically involved and the existence of numerous competing pathways lead to reaction mechanisms rather complicated to elucidate, particularly when transition metal atoms are present. In addition, short-lived intermediates are difficult to detect, which makes the full mechanistic characterization of reactions particularly challenging by using purely experimental techniques.

In the last decades, computational methods have been proven to be tremendously useful for elucidating reaction mechanisms and shaping the current understanding of a broad variety of chemical processes.[1,2] Homogeneous catalysis is probably one of the fields in which the application of computational quantum chemistry methods has been most successful.[3–5] Theoretical calculations allow identifying not only the reaction intermediates but also the species connecting them, namely *transition states* (TSs). The collection of all these structures along a given reaction coordinate can be represented as a function of their relative energies giving rise to the so-called reaction energy diagrams (Figure 1.1).

In a Gibbs energy diagram, the thermodynamics of the reaction is defined as the Gibbs energy difference between the reactants and products ΔG_r. On the other hand, the kinetics is determined by the maximum energy difference between an intermediate and a transition state $\Delta G^\ddagger$ of the diagram. This energy difference, so-called the energetic span (dE),[6] is the apparent activation energy of the entire reaction mechanism.

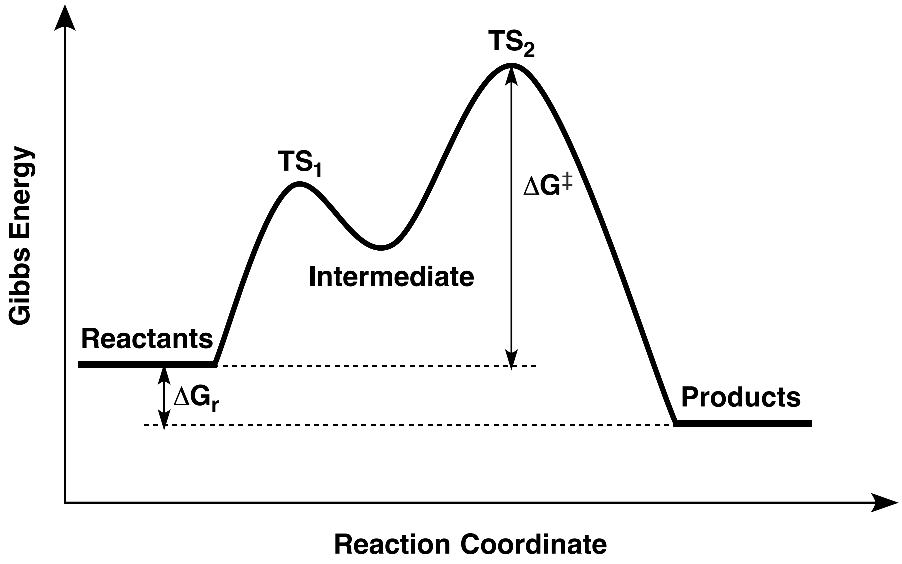

Figure 1.1: Gibbs energy diagram of a model reaction mechanism.

Although theoretically one could think of a vast number of different pathways to go from a given reactants to certain products, in practice only few of them may occur. Hence, mechanistic studies mainly consist in finding the most likely paths associated with the lowest energy pathways at the conditions set for the reaction (pressure, temperature, solvent, etc.).

1.1.2. Catalysis

A catalyst is a substance that increases the rate of a chemical reaction by enabling an alternative mechanism that is more energetically favorable than the one operating in the absence of it. As a result, catalysts allow chemical processes to be carried out under milder conditions and thus more efficiently. They do so by forming bonds with the reactants, thereby allowing these to afford the products more easily. At the end, the generated products detach from the catalyst leaving it unaltered and available for further reactivity. In addition, catalysts may also enhance the selectivity of a reaction by favoring the formation of a single product when several are possible.

On the whole, the steps in a catalytic reaction can be classified into *bonding*, *reaction* and *separation* steps, which constitute the so-called *catalytic cycle* (Figure 1.2).

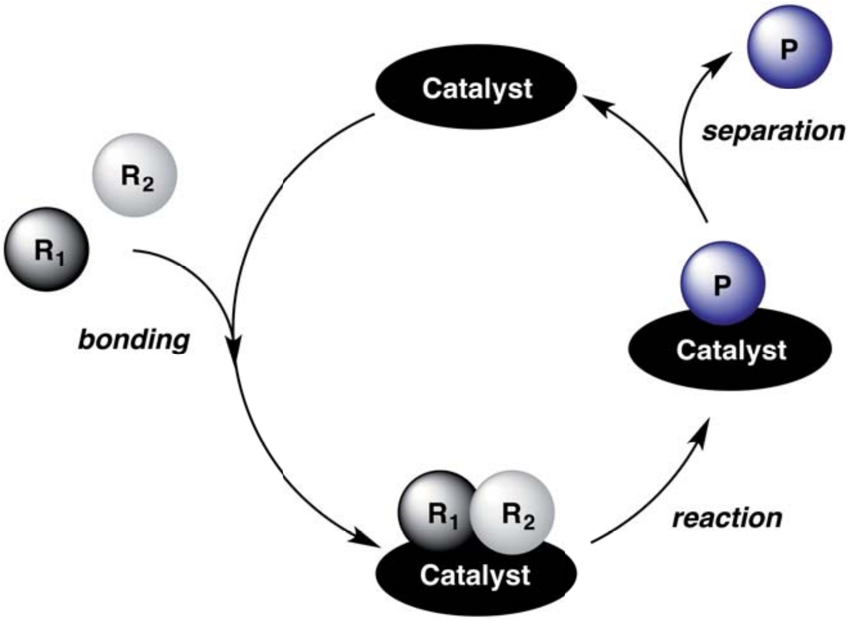

Figure 1.2: Schematic representation of a general catalytic cycle.

A true catalytic cycle, however, is often more complicated that the one shown in Figure 1.2, as the bonding, reaction and separation stages typically involve several elementary steps. Besides, other competing reactions might also take place outside the cycle, which result in inactive species that decrease the reaction rate, even leading to the deactivation of the catalyst in some cases. Thus, obtaining magnitudes that allow measuring their activity and efficiency is crucial for their comparison and the further design of more active catalysts.

The activity of a given catalyst can be quantified by measuring the *reaction rate constant* (k). This magnitude can be theoretically calculated from the Gibbs energy difference between a transition state and reagents, $\Delta G^{\ddagger}$, by means of the *Eyring equation*:[7,8]

$$k = \frac{k_B T}{h} e^{-\Delta G^{\ddagger}/RT} \qquad [1.1]$$

where k_B is the Boltzmann constant, h the Planck constant, R the universal gas constant and T the absolute temperature.

Further, two other quantities are also used: the turnover number (TON), to quantify catalyst robustness, and the turnover frequency (TOF), to quantify catalyst activity. The TON corresponds to the total number of reactant molecules that a catalyst converts into product molecules, while the TOF is the TON relative to the reaction time. These definitions, however, vary slightly depending on the type of catalyst; for example, in heterogeneous catalysis, the TON and TOF are often defined per active site or per gram of catalyst, which is not done in homogeneous catalysis.

As mentioned above, catalysts do reduce the Gibbs activation energy, thus increasing the reaction rate as is shown in Figure 1.3. However, it is important to note that the addition of a catalyst does not affect the thermodynamics of the reaction, as this species is not consumed in the overall process; consequently, the reaction Gibbs energy remains unaltered.

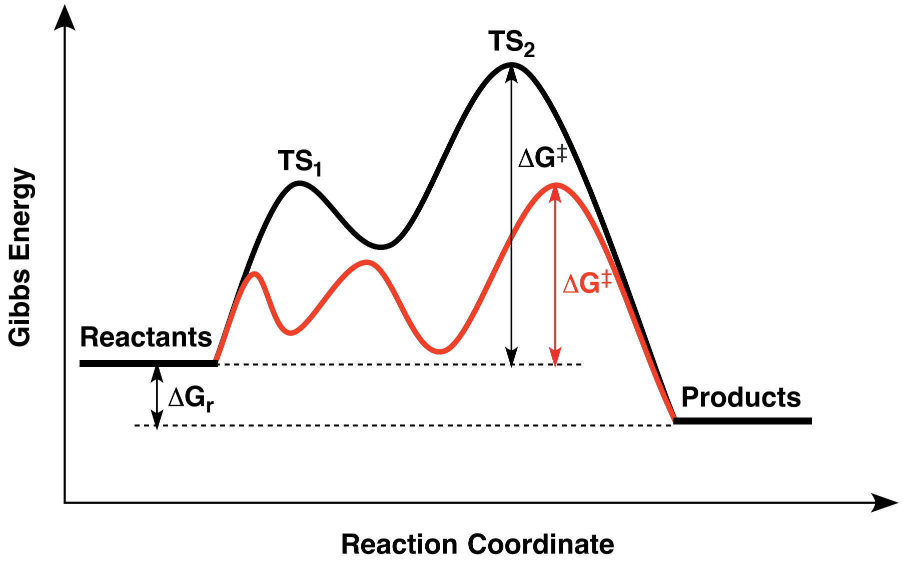

Figure 1.3: Examples of Gibbs energy diagrams for non-catalyzed (black curve) and catalyzed (red curve) reactions.

According to the *Sabatier principle*, the interaction between a good catalyst and the reactants has to be “just right”; that is, neither too weak nor too strong. The reason behind this is that if the interaction is too weak, the substrate will fail in binding the catalyst, and consequently, no reaction will take place. On the other hand, if the interaction is too strong, the catalyst will be blocked by the substrate and/or the product will not dissociate from the catalyst. The Sabatier principle is usually represented graphically by plotting the rate of the reaction as a function of a physical property such as the heat of adsorption of the reactants to the catalyst. These plots are widely known as *volcano plots*, as they usually adopt the shape of a triangle or an inverted parabola passing through a maximum (Figure 1.4).

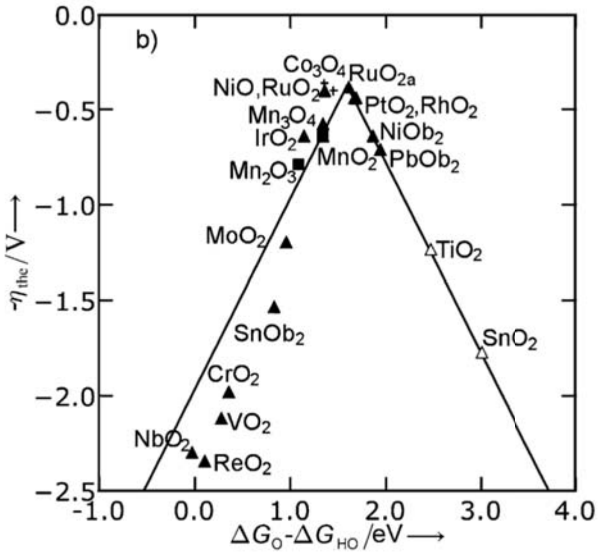

Figure 1.4: Example of a volcano plot representation for the water oxidation reaction catalyzed by different rutile oxides. The negative value of the theoretical overpotential is plotted as a function of the difference between the O and OH adsorption Gibbs energies ($\Delta G_{O*} - \Delta G_{HO*}$). Data has been taken from reference [9].

Catalysts can be classified into three main categories: *homogeneous*, *heterogeneous* and *biological*. These categories comprise a vast variety of catalysts forms, ranging from discrete atoms and molecules to large and complex structures such as zeolites or enzymes. The present thesis focuses on the mechanistic study of oxidation reactions catalyzed by homogeneous and heterogeneous systems. This has allowed us to acquire a broader knowledge of catalysis and to have a general idea of what are the benefits of using one or the other type of catalysts.

In the next sections a detailed description and comparison between homogeneous and heterogeneous catalysts is provided.

1.1.2.1. Homogeneous Catalysis

By definition, homogenous catalysis refers to catalyzed reactions in which both the catalyst and the reactants are in the same phase, most often a liquid. Homogeneous catalysis includes simple acids or bases, organic molecules and organometallic complexes, although the latter two generally receive most of the attention. Strictly speaking, an organometallic complex must contain an M−C bond. Nevertheless, this definition has been generalized to a central metal atom surrounded by any organic (coordination complexes) or inorganic ligand (Figure 1.5).[10,11]

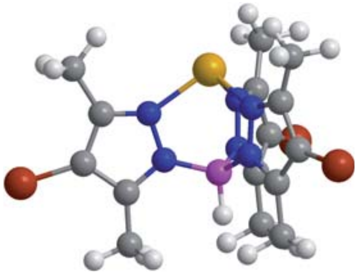

Figure 1.5: Example of one homogeneous catalyst based on a coordination complex of copper studied in this thesis (see Chapters 7 and 8). The metal center is shown in yellow, while the rest of colored atoms correspond to organic ligands (red = Br, gray = C, white = H, blue = N, pink = B).

The most common metals used in organometallic complexes are transition metals due to their ability to easily change their oxidation state during the reaction. The nature of the transition metal and the ligands that constitute the homogeneous catalyst will determine its catalytic activity and robustness. Once the reactants interact with a catalyst, unstable intermediate complexes are usually formed before reaching the final product. A wide variety of catalysts can be obtained from a metal complex simply by changing the electronic or steric properties of the coordinated ligands. As a result, rate enhancements of many orders of magnitude can be obtained with just subtle changes. This has enabled the application of homogeneous catalyst in many fields such as in the fine chemical synthesis,[12] materials science[13,14] or biochemistry.[15]

1.1.2.2. Heterogeneous Catalysis

In contrast with homogeneous catalysis, in heterogeneous catalysis the reactants and the catalyst are in different phases. In most cases, the catalyst is a solid material, while the reactants are in the gas or liquid phase. The most common heterogeneous catalysts can be classified as either metal, metal oxide or zeolite materials (Figure 1.6). These often have well-defined crystal structures, although some of them can also adopt non-crystalline structures (amorphous) or nanoparticles.[16,17] In particular, crystal structures can be simplified to a small set of atoms in the primitive unit cell. There are different types of unit cells which are represented in terms of their lattice parameters, the lengths of the cell edges (a, b, and c) and the angles between them (α, β, γ). Moreover, unit cells can be cut in several planes or facets, described by the three-value Miller index notation (lmn), leading to different stabilities and atomic configurations at the surface.

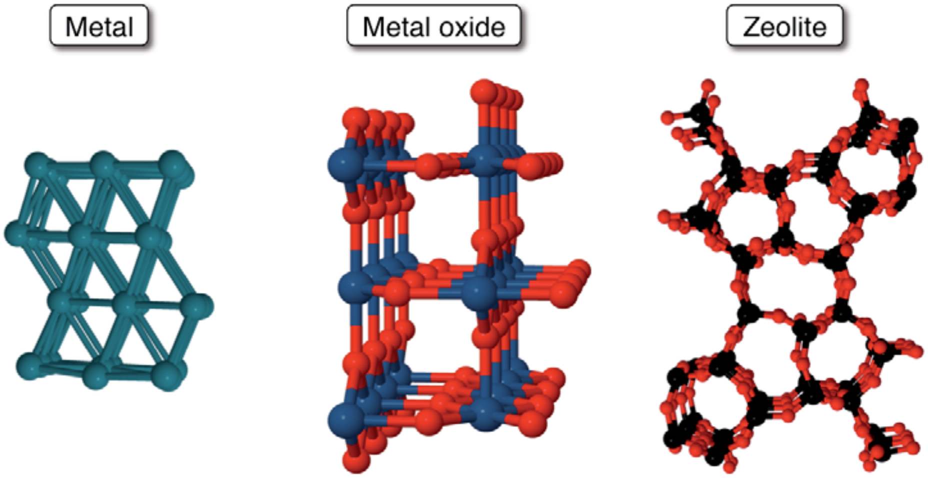

Figure 1.6: Most common types of heterogeneous catalysts.

Given the fact that most solid materials are impenetrable, chemical reactions typically occur at the surface; accordingly, catalytic activity might be different depending on the surface facet or plane exposed. From a computational point, the most stable surface facet of a material is the one that has the lowest energy surface and therefore this is typically chosen for the mechanistic studies.

The most common reaction mechanisms in heterogeneous catalysis involve the adsorption of at least one reactant onto a surface active site; then this intermediate species reacts leading to the reaction products, which desorb from the surface closing the catalytic cycle. In the particular case of bimolecular reactions, two main reaction mechanisms are known: the Langmuir-Hinshelwood and the Elay-Rideal (Figure 1.7). In the former, the two reactants adsorb on neighboring surface sites and then undergo a bimolecular reaction before desorbing from the surface. In contrast, in the Elay-Rideal mechanism, only one reactant is adsorbed onto the surface, which subsequently interacts and reacts with the other reactant in the gas phase.

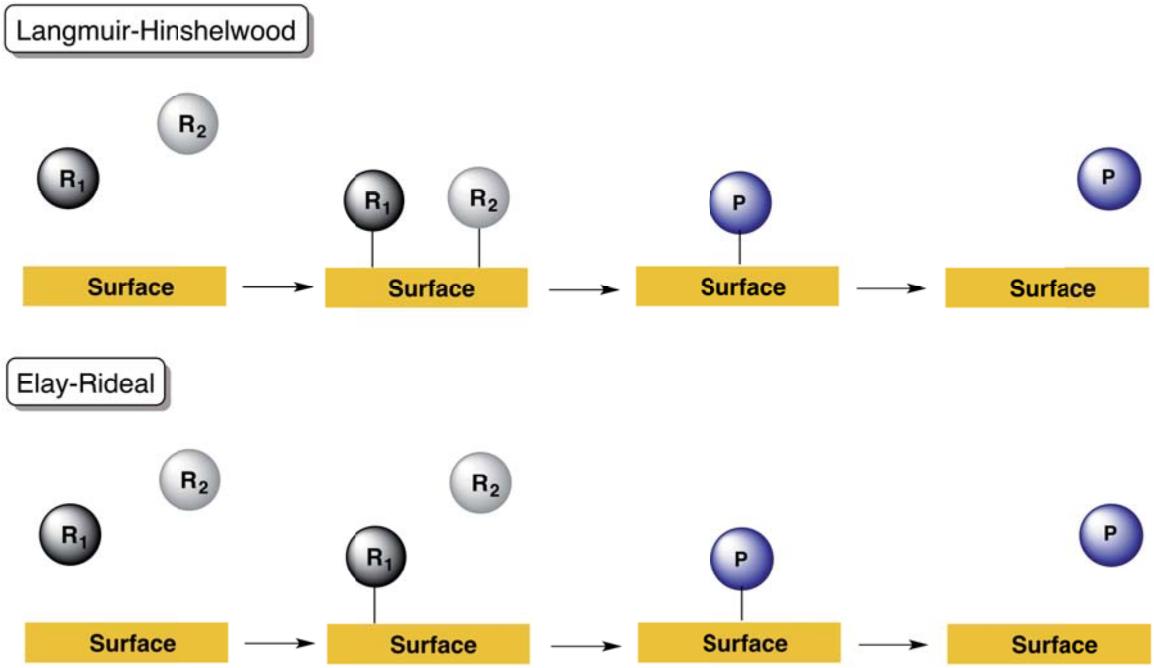

Figure 1.7: Bimolecular reaction mechanisms in heterogeneous catalysis.

1.1.2.3. Homogeneous *vs.* Heterogeneous Catalysis

In principle, there should not be any preference in using either a homogeneous or heterogeneous catalyst, and the choice of one or the other should be rather dictated by the chemical process of interest. As a matter of fact, the first industrial catalyzed reaction dates from 1750 and was the oxidation of SO_2 to SO_3 using nitrogen monoxide as a homogeneous catalyst. Other examples of homogeneous catalyzed reactions include the hydroformylation by rhodium-based catalysts[18,19] the Ziegler-Natta polymerization,[20,21] the Wacker process[22,23] and the Fischer-Tropsch reaction.[24] Nevertheless, in practice, heterogeneous catalysts have been more widely employed in industry, mainly because they are in a distinct phase than the reaction medium, which makes easier the separation and recycling processes. Some of the most relevant applications of heterogeneous catalysts are the production of methanol from CO and H_2 (syngas),[25,26] the ammonia synthesis (Haber process)[27] and the oil cracking. [28,29]

In Table 1.1, a list comparing the main strengths and weaknesses of both types of catalysts is presented. It is important to note that, in general, the major limitations of homogeneous catalysts appear to be the major advantages of heterogeneous ones.

Table 1.1: Comparison of the main advantages/disadvantages of homogeneous *versus* heterogeneous catalysts.

Property	**Homogeneous**	**Heterogeneous**
Active site	**Well-defined**	Not well-defined
Selectivity	**High (single active site)**	Low (multiple active sites)
Reaction mechanisms	**Well understood**	Poorly understood
Catalyst Tunability	**Easy**	Difficult
Diffusivity	**High**	Can be problematic
Heat transfer	**Easy**	Can be problematic
Product separation	Generally problematic	**Easy**
Catalyst recovery	Difficult and expensive	**Easy and cheap**
Thermal stability	Mild	**High**

One of the most evident advantages of homogeneous catalysts over heterogeneous is that, in the former the active sites are generally more well-defined than in the later. Consequently, the characterization of homogeneous catalysts and the elucidation of their reaction mechanisms are much simpler compared to the heterogeneous ones. Furthermore, the well-defined structure of homogeneous catalysts makes their geometric and electronic properties easier to tune. Other benefits for homogeneous catalysts are for example their high levels of diffusivity and heat transfer.

On the other hand, heterogeneous catalysts are much easier to separate from products and reactants and to recycle, than homogeneous systems. In fact, these are the main reasons that make heterogeneous catalysts more suitable for the industry. Besides, heterogeneous catalysts are less affected by the reaction temperature than homogeneous ones, in which the temperature is constrained by the presence of the solvent and by their own thermal stability.

Overall, both homogeneous and heterogeneous catalysts have advantages and disadvantages, and usually the limitations of ones appear to be the main strengths of the others and vice versa. Hence, the combination of two types of catalysts into a hybrid type catalyst has recently emerged as a promising alternative in order to benefit from both.[30] Two successful examples that use this strategy are an Ir-based HEDTA catalyst supported on TiO_2[31] and a dimeric Ir complex anchored on of tin-doped indium oxide nanoparticles.[32]

1.2. Oxidation Reactions

As mentioned in the opening paragraph of this first chapter, the present Ph.D. thesis focuses on the computational study of reaction mechanisms in the framework of oxidative catalysis. More specifically, we have investigated the catalytic oxidation of water and covalent bonds with carbon, including C−H, C−C and C=C, which are among the most relevant reactions in this research field.

Given the fact that all the reactions explored have been widely investigated and a large amount of data has been reported about them, the following sections are not intended to be exhaustive. They only aim at giving a general overview paying particular attention to the most relevant studies on these reactions. Thus, the main goal of this thesis is to achieve a fundamental understanding of these chemical processes. This knowledge can be used in the near future to develop more active, robust and sustainable catalysts for this chemical processes.

1.2.1. Water Oxidation

Nowadays the major part of the global energy supply is covered by the depleted fossil fuels reservoirs, which are the primary contributors to global warming. Consequently, there exists a strong interest in generating electric energy from environmentally friendly and renewable sources able to meet the energy needs in the future. Solar and wind energies are among the most abundant and potential readily available sources; however, they are not constant and reliable throughout the day and are often concentrated on remote areas. Therefore, to provide integrated solutions, such technologies must be coupled with advanced energy conversion and storage techniques.[33-36] In this context, electrochemistry plays a central role, as it allows the reversible transformation of electricity into chemical energy (in electrolysis cells), thereby enabling the storage of energy in the form of chemical bonds. This stored energy can be subsequently used to cover the energy deficit at times when the supply does not meet the demand by converting it into electrical energy through spontaneous electrochemical reactions, which occurs in fuel cells (Figure 1.8).

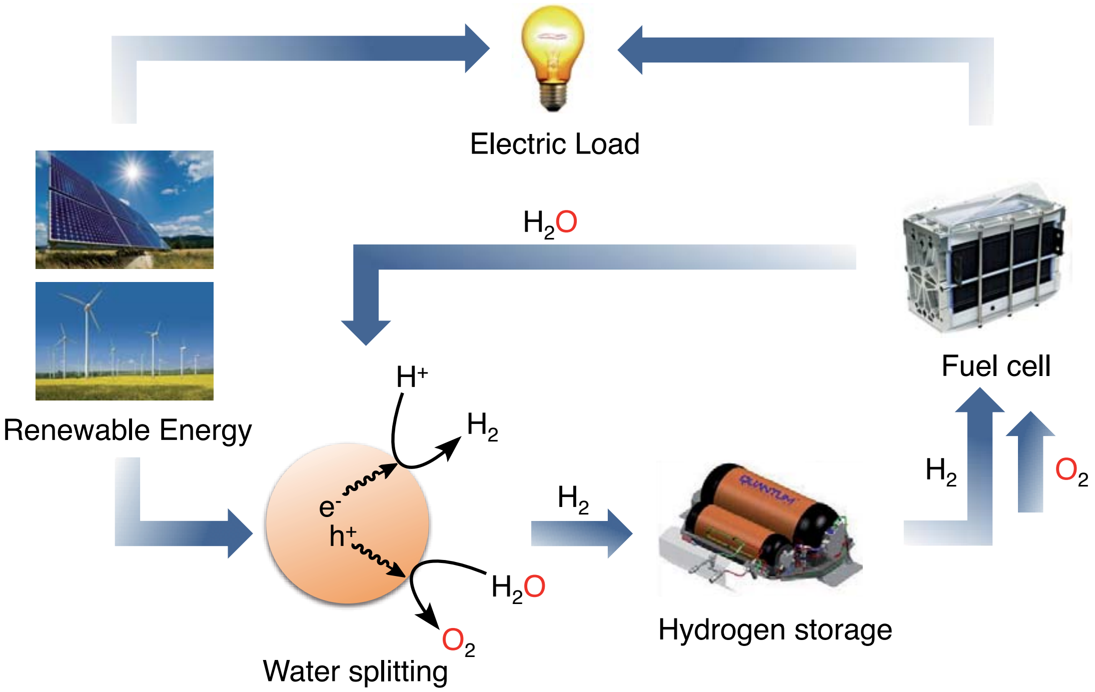

Figure 1.8: Conversion of solar energy into electricity by means of the water splitting reaction.

One of the reactions that has attracted more attention for electrolysis cells is the water splitting (Eq. 1.2). In this process, water is decomposed into molecular oxygen and hydrogen, requiring an overall potential (ΔE^0) of +1.23 V with respect to the standard hydrogen electrode (SHE), at pH = 0.

$$2H_2O_{(l)} \longrightarrow O_{2(g)} + 2H_{2(g)} \qquad \Delta E^0 = +1.23 \text{ V} \qquad [1.2]$$

The positive value of ΔE^0 indicates that water dissociation is thermodynamically unfavorable; that is, this reaction cannot occur without the input of an external energy source. This can be either a sacrificial oxidant such as cerium(IV) ammonium nitrate (CAN)[37,38] or $NaIO_4$,[39,40] or an external applied potential. In practice, however, a much higher potential is needed to drive water splitting. This difference between the real potential and the thermodynamic potential (1.23 V) is called overpotential (η). Thus, a higher overpotential means a higher energy loss in the water oxidation process. One way to lower the overpotential is to develop catalysts with a high (photo)-electrocatalytic activity.

The water splitting reaction can be divided in two half reactions, namely proton reduction and water oxidation, also known as hydrogen and oxygen evolution reactions, respectively (Eqs. 1.3 and 1.4).

$$4H^+_{(aq)} + 4e^- \longrightarrow 2H_{2(g)} \qquad E^0 = 0.00 \text{ V} \qquad [1.3]$$

$$2H_2O_{(l)} \longrightarrow O_{2(g)} + 4H^+_{(aq)} + 4e^- \qquad E^0 = +1.23 \text{ V} \qquad [1.4]$$

Platinum-based catalysts are known to catalyze the hydrogen evolution reaction with high rates, although it remains challenging to develop other catalysts based on cheaper metals.[41,42] On the other hand, the water oxidation reaction is still hampered by the lack of efficient catalysts able to overcome the sluggish kinetics associated with this transformation.

In nature, water is catalytically oxidized in the photosynthesis process by the $CaMn_4O_5$ cluster in the Oxygen-Evolving Complex (OEC) of Photosystem II (PSII),[43] which is found in the thylakoid membranes of green plants. Inspired by this natural system, scientists have focused for several decades on the development of artificial photosynthetic catalysts. A wide variety of catalysts capable of mediating the four-electron-four-proton oxidation process have been developed, including monometallic[44,45] and bimetallic[46–50] complexes, polioxometalates[51,52] and heterogeneous systems.[53,54] Some of them are based on manganese as the $CaMn_4O_5$ cluster,[46,47,55] although those based on noble metals such as Ru[45,56–60] and Ir[61–64] are currently among the most active ones. All these catalytic systems, however, are still far to be scaled up to the industrial level for some of the following reasons: poor activity, low stability, small current densities and/or scarcity and high cost of their metal constituents. As an alternative, recent studies have revealed that earth-abundant metals,[65] such as Ni,[66] Fe[67–69] Co,[70] and Cu[71] display encouraging activity in an alkaline environment, and are therefore promising candidates to replace the above-mentioned precious metal-based catalysts.

1.2.1.1. Reaction Mechanisms

Extensive research has been devoted toward elucidating and understanding the fundamental steps of water oxidation reaction. In particular, the step that has received greater attention corresponds to the formation of the O−O bond, since it has been found in many cases to be the rate-determining step of the entire process.[72]

The two main reaction mechanisms proposed for the O−O bond formation, using both homogenous and heterogeneous catalysts, are the water nucleophilic attack (WNA)[73–76] and the direct coupling (DC)[77–79] mechanisms (Scheme 1.1). Which one of the two is more feasible is still a subject of debate and strongly depends on the nature of the catalyst employed.[72,80]

The WNA mechanism can be understood as an acid/base process in which an M=O moiety acts as a Lewis acid by accepting two electrons from an incoming water molecule, resulting in a hydroperoxo intermediate. In this process, one of the protons of the water molecule is released either to the reaction medium[75,81] or to a Lewis base center from the same catalyst[82,83] (Scheme 1.1). Finally, the hydroperoxo species undergoes further oxidation to liberate O_2. On the other hand, the DC mechanism consists in a radical coupling between two terminal oxygen atoms from vicinal M=O moieties. It leads to a bimetallic peroxo compound with each metal reduced by one electron that ultimately releases O_2. This mechanistic hypothesis has been considered in the design of bimetallic catalysts, many of which use cofacial or conformationally locked structures to favor this direct coupling.

Scheme 1.1: The two main reaction mechanisms proposed for water oxidation in bimetallic systems.

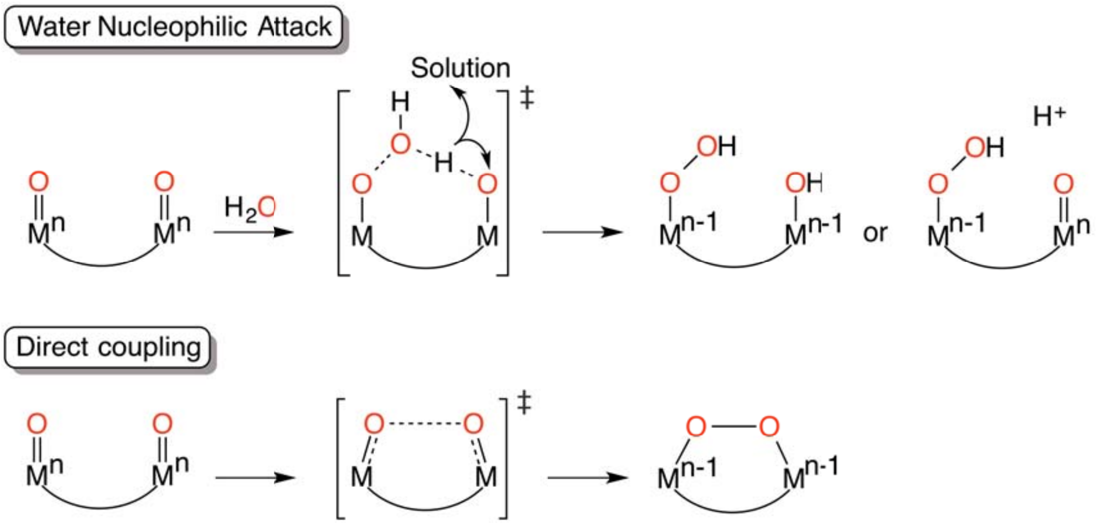
Water Nucleophilic Attack
Solution
H₂O
‡
H⁺
or
Direct coupling
‡
M
Mⁿ
Mⁿ⁻¹
OH
O

1.2.2. C=C Oxidation

The oxidation of hydrocarbons containing C=C bonds is a powerful synthetic strategy to convert hydrocarbon feedstock into high added-value chemicals such as ketones, epoxides or aldehydes (Figure 1.9). Molecular oxygen is the most desirable oxidant agent, however, the selective partial oxidation of C=C bonds with O_2 is difficult to control and usually results in complete combustion to CO_2 and H_2O.[84] To avoid this, transition metal catalysts have been developed to activate O_2 on a controlled manner.

Pharmaceuticals
Acetone
Paints
Perfumes
Adhesives

Figure 1.9: Examples of industrial applications of ketones, epoxides and aldehydes.

In industry, the two main catalytic systems to oxidize alkenes with O_2 are the Pd/Cu-catalyst[85] and Ag-based catalysts.[86] The Pd/Cu-catalyst is used in the homogeneous oxidation of terminal alkenes to methyl ketones by O_2, extensively known as the Wacker process, while heterogeneous Ag catalysts are applied for the epoxidation of alkenes, such as in the production of glycol and ethylene oxide (Scheme 1.2).

Scheme 1.2: Formation of methyl ketones by the Wacker process and formation of ethylene oxide catalyzed by supported Ag.

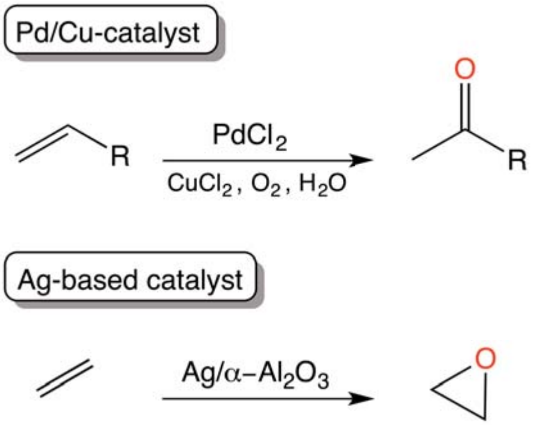

In the last years, Rh[87] and Ir[88] catalysts have been also proven to catalyze the alkene oxidation reaction. With the appropriate choice of ligands, these metals enable the oxidation of alkenes in a stepwise manner.[89] This has allowed the experimental characterization of intermediates, thus providing some guidelines for the elucidation of the reaction mechanism.

1.2.2.1 Reaction Mechanisms

Among all the existing metal-catalyzed olefin-oxidation reactions, in this thesis we have focused on the oxygenation of olefins directly coordinated to rhodium and iridium centers.[90] Several Ir and Rh-based complexes have been reported in the literature, giving rise to the generation of a broad variety of oxidized products (Scheme 1.3).

Scheme 1.3: Reaction products obtained in the oxygenation of M−ethene complexes.

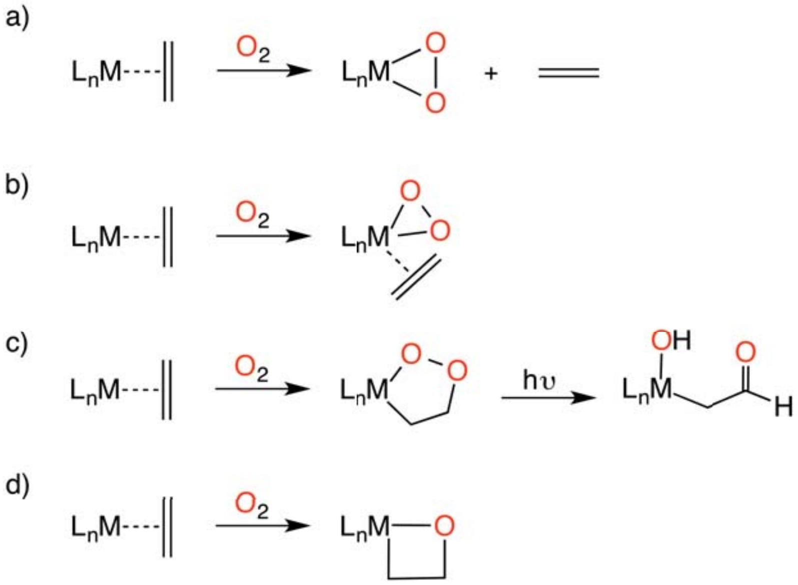

The formation of peroxo species (Scheme 1.3a) is more common with Rh complexes than with Ir ones. This reaction typically involves the dissociation of the olefin as is the case of the $[(Me_3tpa)Rh^I(ethane)]^+$ (tpa = tris(2-pyridylmethyl)amine)) complex.[91] However, olefin displacement can be prevented by introducing a chelate ligand such as cyclooctadiene (cod), thus allowing the selective oxygenation of some Rh complexes.[92] On the other hand, the formation of peroxo-ethane species is more common by using Ir-based complexes in aprotic solvents (Scheme 1.3b). Some examples are: $[(PPh_3)_2(Cl)Ir^I(ethane)_2]$,[93] $[(Me_2bpa\text{-}Me)Ir^I(ethane)]^+$ (bpa = bis(2-pyridylmethyl) amine))[91] and $[(Me_3tpa)Ir^I(ethane)]^+$.[91]

3-metalla-1,2-dioxolane oxidation products (Scheme 1.3c) have been detected and isolated[94,95] mainly in aprotic solvents or air, where both oxygen atoms are derived from the same O_2 molecule. One example is the reaction of the $[(tpa)Rh(ethane)]^+$ solid complex with O_2.[95] As is shown in Scheme 1.3c, 3-metalla-1,2-dioxolanes can also evolve to a stable hydroxy-ß-oxoethyl species under thermal or photochemical activation or source of protons, through O−O cleavage and ß-hydrogen migration.[96] Finally, 2-metalla-oxetanes (Scheme 1.3d) are usually obtained in the presence of H_2O_2 as oxidant. A well-known example is the 2-iridaoxetane product obtained by

Klemperer and co-workers from the $[(P_3O_9)Ir^I(cod)]^{2-}$ complex.[97]

Overall, Scheme 1.7 shows how oxidation of olefins mediated by metal complexes can give rise to a whole variety of organic products. The final outcome of these reactions depends strongly on the nature of the metal center, the ligands and the reaction conditions. For instance, Ir complexes are usually less reactive toward oxygenation than Rh ones, which make the former more suitable for mechanistic studies. In addition, Ir has a stronger affinity for olefins than Rh due to its better π-donor electron ability.[98] Consequently, the loss of ethene from Ir is slower than from Rh. When it comes to the reaction conditions, the use of peroxides as oxidants or protic solvents typically favors mono-oxygenation reactions that results in reactive 2-metallaoxetane intermediates.[99,100] In contrast, the use of dioxygen in aprotic solvents or gas phase, is believed to promote the formation of 3-metalla-1,2-dioxolanes.[96] Due to the strong oxidant conditions required in all these reactions, oxidation-resistant ligands are needed such as multidentate nitrogen donor ones.

1.2.3. C−H Oxidation

The pursuit of new strategies to selectively convert hydrocarbons into valuable oxy-functionalized organic compounds is one of the most active research topics in chemistry. Designing an efficient process to selectively activate C−H bonds[101] would be of great importance in the synthesis of fine chemicals, and to displace petroleum by more abundant and cheap hydrocarbons, such as methane, to produce methanol for its use in combustion engines and fuel cells.[102] However, the major challenge is the high energy required to cleave the inert and strong C−H bonds (binding energy, BDE $\approx$ 100 $kcal \cdot mol^{-1}$), which can be only achieved by using strong oxidizing reagents under harsh conditions. On this issue, Mayer showed that the C−H bond BDE depends linearly on the activation energy of this bond.[103,104] Indeed, the use of catalysts that weaken the C−H bond (Figure 1.10) has been shown to allow the reaction to be conducted under much milder conditions.[105,106] Besides, it is important to take into account that these catalysts need also to be selective in order to avoid overoxidation of the desired products.[107–109]

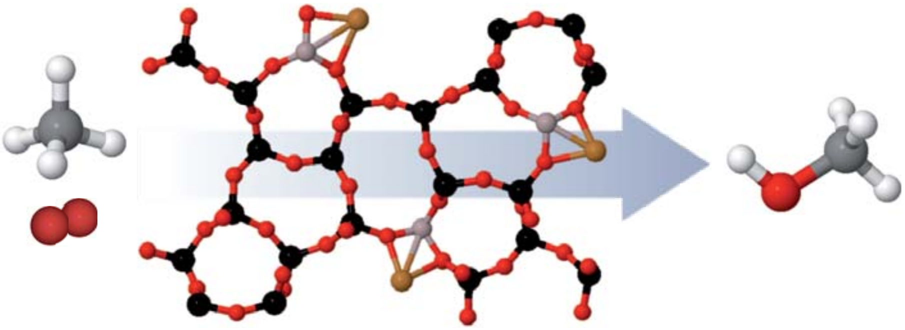

Figure 1.10: Example of the partial oxidation of methane to methanol catalyzed by a Cu-doped ZSM-5 zeolite.

In nature, oxidation of alkanes is effectively carried out using molecular oxygen, the most environmentally benign, non-toxic and available oxidizing agent. Significant efforts have been undertaken to understand how nature performs these transformations[110–112] and to engineer selective and stable biomimetic alkane hydroxylases.[113,114] Nevertheless, their industrial application is still a long way from achieving the activity and selectivity that enzymes provide in nature.

Two of the most relevant C−H oxidation processes are those involving benzene and methane. Ideally, these processes would involve a single reaction in which one oxygen atom, provided by a benign oxidant like O_2 or H_2O_2, would be inserted into a C−H bond of the substrate. In reality, however, these processes in industry require several consecutive reactions with overall low efficiencies.

Phenol is one of the most important intermediates in the chemical industry. Its synthesis is mainly carried out through the so-called *cumene hydroperoxide process* (Scheme 1.4), which consists of three main chemical steps: propylation of benzene to produce cumene, the oxidation of cumene to cumene hydroperoxyde with air, and Hock rearrangement. However, this strategy only yields 5% of phenol and an equimolar amount of acetone is generated as byproduct.

Scheme 1.4: Cumene process for the production of phenol.

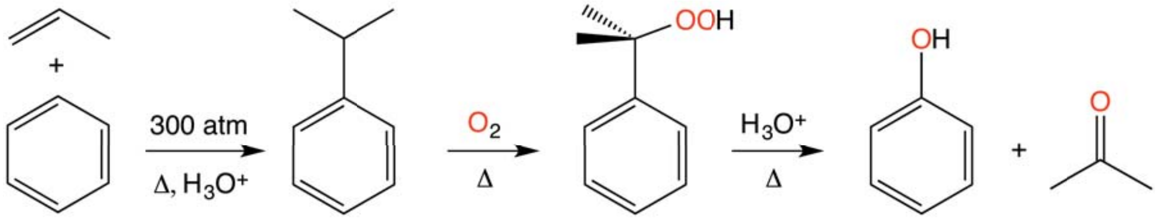

Even more challenging is the methane to methanol oxidation reaction. The current industrial method is a multistep process and consumes significant amounts of energy, which makes it rather expensive. More specifically, it involves the steam reforming of methane to a mixture of carbon monoxide and hydrogen (syngas),[115] followed by a high pressure catalytic process that finally gives rise to methanol (Eqs. 1.5 and 1.6).

$$CH_{4(g)} + H_2O_{(g)} \xrightarrow{Ni,\ \Delta} CO_{(g)} + 3H_{2(g)} \qquad [1.5]$$

$$CO_{(g)} + 2H_{2(g)} \xrightarrow{Cu/ZnO} CH_3OH_{(g)} \qquad [1.6]$$

1.2.3.1 Reaction Mechanisms

C–H bond cleavage by means of a transition metal complex, L_nM, generally involves two synergic transfers of electron density: σ-donation from the bonding σ(C–H) molecular orbital (MO) on the substrate into a vacant orbital on L_nM and π-backdonation from an occupied MO on L_nM into the antibonding σ*(C–H) MO on the substrate.[116,117]

Several reaction mechanisms have been proposed for metal catalyzed C–H bond activation. These mechanisms can be classified in two main groups, depending on whether an M–C σ-bond is formed or not. The most relevant mechanisms involving the formation of the M–C bond are: the oxidative addition, the σ-bond metathesis, the electrophilic aromatic substitution and the 1,2-addition (Scheme 1.5).

Scheme1.5: Main reaction mechanisms for C–H oxidation involving the formation of an M–C bond.

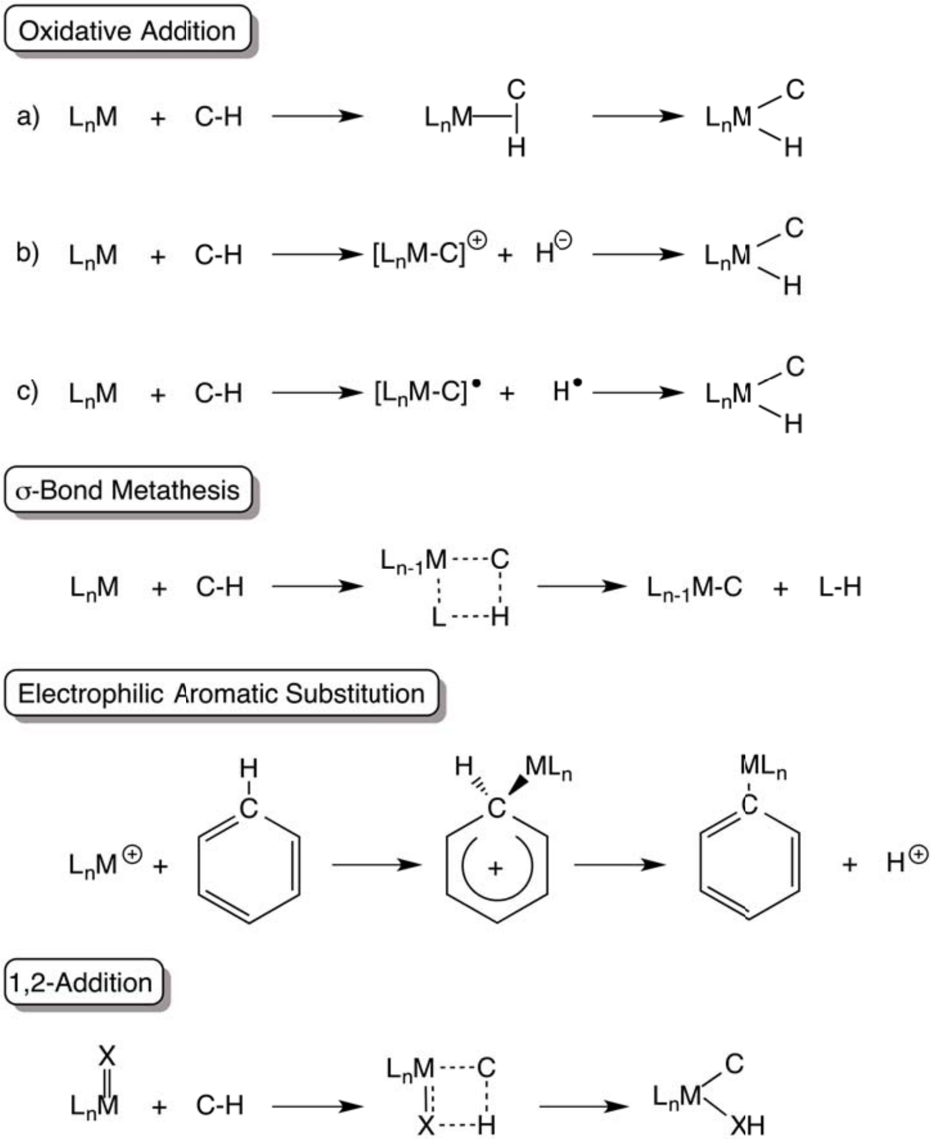
Oxidative Addition
a) L_nM + C-H → L_nM—C—H → L_nM C H
b) L_nM + C-H → $[L_nM\text{-}C]^{\oplus}$ + $H^{\ominus}$ → L_nM C H
c) L_nM + C-H → $[L_nM\text{-}C]^{\bullet}$ + $H^{\bullet}$ → L_nM C H
σ-Bond Metathesis
L_nM + C-H → $L_{n-1}M$ C L H → $L_{n-1}M$-C + L-H
Electrophilic Aromatic Substitution
$L_nM^{\oplus}$ + H C → H ML_n C + → ML_n C + $H^{\oplus}$
1,2-Addition
X L_nM + C-H → L_nM C X H → L_nM C XH

Among the mechanisms shown in Scheme 1.5, the oxidative addition is the most common one. It entails the cleavage of the C–H bond leading to the formation of M–H and M–C bonds. There are several multistep reaction pathways (Scheme 1.5) proposed to describe this process, although in all of them the metal is formally oxidized in two units. Thus, this mechanism is typical for electron-rich late transition metals, such as Pd and Pt.[118] For early transition metals with d^0 electronic configuration, an oxidative process is not possible, and the preferred mechanism is σ-bond metathesis,[119] which consists in a concerted L ↔ C exchange between the M−L and the C−H bonds. A similar mechanism is the electrophilic aromatic substitution, observed for late transition metals in a strongly polar medium, in which the M−C bond is formed by addition of the substrate to the metal complex and elimination of one proton. The last mechanism involving the formation of an M−C bond is the 1,2-addition,[120,121] in which the C−H bond is added to an unsaturated M=X bond, where X is generally an amido or alkylidene group.

For C−H activation reactions without formation of M−C bond, there are mainly two proposed mechanisms: electrophilic aromatic substitution and rebound (Scheme 1.6). Both involve metaloxo species[122] and the formal oxidation of the substrate due to the formation of a C−O bond. In the electrophilic aromatic substitution, the aromatic system adds to the oxo ligand, leading to the generation of a zwitterionic species.[123] In contrast, in the rebound mechanism, the oxo ligand abstracts an H atom yielding an organic radical species. After the homolytic cleavage of the C−H bond, the radical attacks the M−OH moiety leading to an alcohol product coordinated to the metal center.[124]

Some examples of reported metal oxo moieties that promote the C−H oxidation are: $[\mathrm{Mn^{IV}O}]^{2+}$,[125,126] $[\mathrm{Ru^{IV}O}]^{2+}$[127] and $[\mathrm{Fe^{IV}O}]^{2+}$.[128] In fact, the latter has been shown to be the reactive core in some of the most active oxidizing systems, including the Fenton reagent[129] biomimetic iron complexes, heme and non-heme enzymes,[130] and iron-containing zeolites.[131]

Scheme 1.6: Reaction mechanisms for C−H activation without formation of a M−C bond.

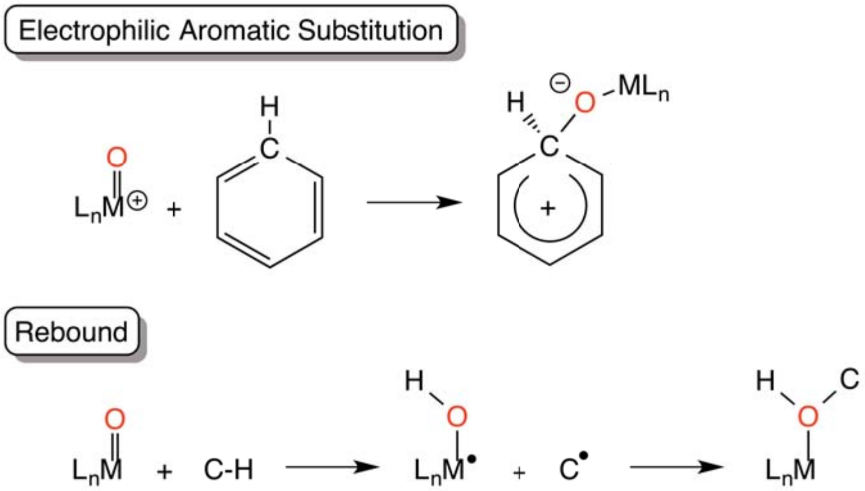

1.2.4. C−C Oxidation to C=C

Alkenes are the most versatile feedstock in chemical industry because they have a wide range of applications; for example, in the manufacture of plastics, polymers or as raw materials in the production of add-value chemicals (Figure 1.11).[132] However, these compounds are far less naturally abundant than alkanes. Hence, the catalytic dehydrogenation of alkanes is the most direct and potentially the most economical route to produce alkenes.[133,134]

PVC plasticizers Detergents Textiles Lubricants Packaging

Figure 1.11: Examples of industrial applications of alkene derivatives.

At present, alkenes are mainly produced in industry by hydrocarbon cracking. This process consists in the breakdown of heavy hydrocarbons into simpler molecules such as light alkanes and alkenes, which operates at high temperatures (500-900°C) and, in some cases, in the presence of solid acid catalysts. Nevertheless, this methodology is limited by its low selectivity, yielding mixtures of ethylene, ethylbenzene and other hydrocarbons.[135] The harsh conditions required for this reaction are due to the inertness of the C−H bond and also because it is the reverse of a pericyclic reaction via a 4-membered ring transition state, which is typically hampered by a high energy barrier.[136–138] A way to overcome these issues is to employ an efficient catalyst that allows an alternative path to the direct reaction and to use a sacrificial hydrogen acceptor (SA) to keep the catalyst in its active form.

Several transition metal catalysts based on Re,[139] Ir [140,141] and Rh [142] have been found to catalyze such reaction at relatively low temperatures (100-150°C). Among these catalysts, pincer-ligated iridium complexes have been proven to be by far the most active due to their high thermal stability.[143,144] The use of these pincer iridium catalysts enabled the efficient acceptorless dehydrogenation reaction under reflux conditions,[145] which does not require a sacrificial hydrogen acceptor.

1.2.4.1. Reaction Mechanisms

The catalytic dehydrogenation of an alkane requires the sequential cleavage of two C−H bonds and the concomitant formation of a C=C bond. The generally accepted mechanism for this reaction starts with the oxidative addition of a C−H bond from the alkane to the metal fragment, yielding a hydride alkyl complex (Scheme 1.7a). From this species, a β-H elimination takes place leading to the formation of the corresponding alkene and L_nMH_2. Finally, in order to recover the catalyst, a sacrificial hydrogen acceptor (SA) or reflux conditions, are required to abstract the two hydrogen atoms from the L_nMH_2 species. Besides, the catalytic dehydrogenation can be also accomplished by $L_nM{=}O$ active species.[125] In this case the reaction starts with a radical H abstraction from one of the sp^3 C−H bonds resulting in the formation of the $L_nM{-}OH$ intermediate. This species promotes a second H abstraction from the adjacent C−H bond to give $R_2C{=}CR_2$ and $L_nM{-}OH_2$, which will be reoxidized to recover the active oxo metal species (Scheme 1.7b).

Scheme 1.7: General dehydrogenation of alkanes to alkenes catalyzed by L_nM and $L_nM{=}O$.

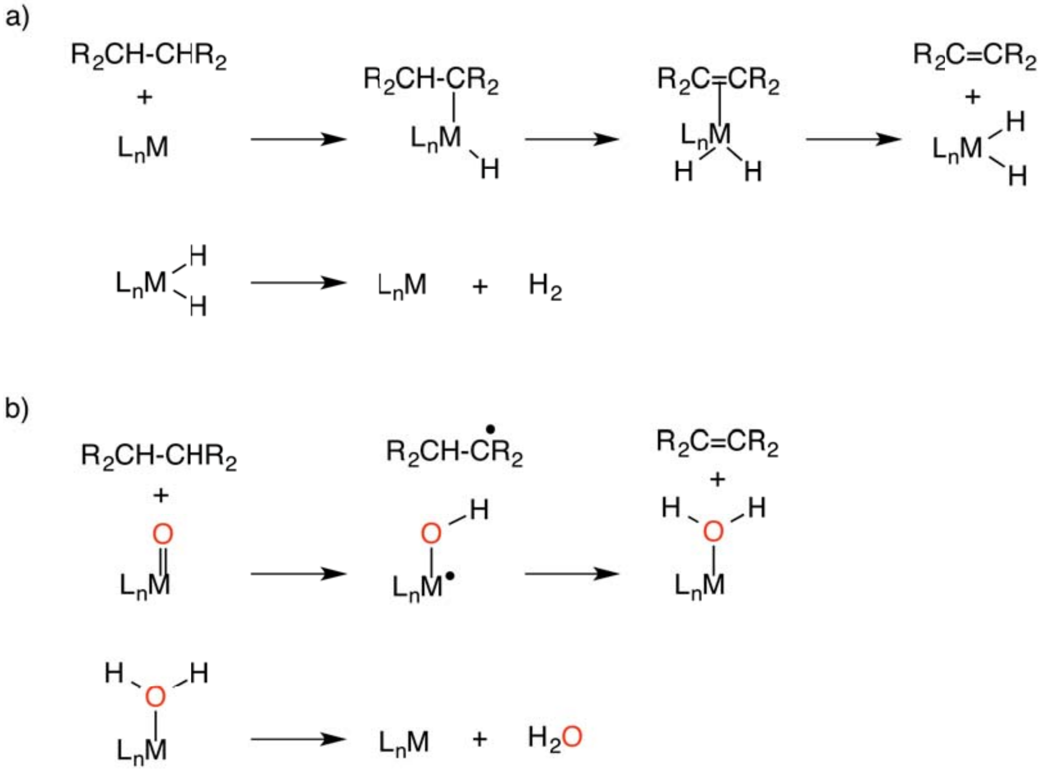
a)
R2CH-CHR2
+
LnM
R2CH-CR2
LnM
H
R2C=CR2
LnM
H
H
R2C=CR2
+
LnM
H
H
LnM
H
H
LnM
+
H2
b)
R2CH-CHR2
+
O
LnM
R2CH-CR2
O
H
LnM
R2C=CR2
+
H
O
H
LnM
H
O
H
LnM
LnM
+
H2O

"Always using the same methods is not God's way."

Sunday Adelaja

2

Computational Details

The aim of this chapter is to provide a general overview of the computational methods employed throughout this thesis. First of all a brief introduction to Quantum Mechanics is given, with special focus on the Density Functional Theory (DFT) and how this methodology is applied to the study of both discrete and periodic systems. In addition, the following chapters include a more specific description of the particular methods that have been used to study each reaction mechanism.

2.1. Quantum Mechanics

According to Quantum Mechanics, any system is fully described by its *wave function* (Ψ). The wave function depends on the time and the coordinates of all particles in the system (Eq. 2.1), although a common approach in computational chemistry is to consider the time-independent Ψ.

$$\Psi(x,\mathrm{t}) = \mathrm{e}^{-\frac{\mathrm{iEt}}{\hbar}}\Psi(x) \qquad [2.1]$$

Thus, most methods used for the study of chemical reactions are based on the solution of the *time-independent Schrödinger equation*[146]:

$$H_{tot}\Psi(x) = E_{tot}\Psi(x) \qquad [2.2]$$

where H_{tot} is the *total Hamitonian* operator and $\Psi(x)$ are the *eigenstates* of the Hamiltonian, whose *eigenvalues* E_{tot} correspond to the total energies of those states. At this point, in order to simplify the resolution of the Schrödinger equation for molecular systems, the *Born-Oppenheimer approximation* is applied. The basis of this approximation is the fact that nuclei are much heavier than electrons and thus, they move at much lower speeds. Hence, it is reasonable to consider the electrons of the molecule moving in a field of fixed nuclei. This approximation results in the simplification of the H_{tot} to the *electronic Hamiltonian* (H_{el}), which is defined as:

$$H_{el} = T_{el} + \left(V_{ne} + V_{ee} + \underbrace{V_{nn}}_{Const}\right) = T_{el} + V \qquad [2.3]$$

T_{el} stands for the kinetic energy of the electrons, V_{ne} for the Coulomb attraction potential between the electrons and the nuclei, and V_{ee} and V_{nn} for the Coulomb repulsion potential between electrons and nuclei, respectively. By applying this Hamiltonian to the electronic wave function, the electronic states of the molecule are obtained by solving the equation:

$$(T_{el} + V)\Psi_{el}(R,r) = U_n(R)\Psi_{el}(R,r) \qquad [2.4]$$

being U_n the sum of the electronic energy (both kinetic and potential) and the

Coulomb repulsion between the nuclei, for a set of fixed nuclear coordinates.

This Born-Oppenheimer potential, also referred to as *adiabatic potential*, can be calculated for a large number of nuclear positions yielding a *potential energy surface* (see section 2.3.3). However, except for very simple cases like H_2^+, the electronic Schrödinger equation cannot be solved exactly when it comes to many-electron systems, due to the *many–body interacting problem*. To tackle this problem, several methods have been developed, which can be classified into two classes: methods based on the wave function (*ab initio*) and methods based on the electron density.

Among the first class of methods, probably the most relevant one is the *Hartree-Fock* (HF) method,[146] since it is able to predict many of the physical and chemical properties of the system and also constitutes the starting point of more elaborated and accurate methods including CCSD(T), which is the "gold standard" in computational chemistry. The essence of the HF approximation is to avoid the complicated many-electron problem by considering each single electron on an average electron-electron repulsion potential. Its main drawback is that this method does not consider the electron motion to be correlated. Electron correlation is considered in the so-called post Hartree-Fock methods, including *Configuration Interaction* (CI), *Coupled Cluster* (CC) and *Many Body Perturbation Theory* (MBPT). Moreover, the electronic HF wave function still relies on $4N$ variables, where N is the number of electrons.

In this thesis, however, all the calculations have been performed using the *Density Functional Theory* (DFT), which is based on the calculations of the electron density of the system.[147] This method provides a very good compromise between accuracy and computational cost. Further, it is also a cheap alternative for introducing electron correlation effects into the solution of the electronic Schrödinger equation. The calculation of electronic properties from the electron density, instead of from the wave function, is more straightforward because it only depends on the three spatial coordinates (x,y,z). The next section is devoted to describe in more detail this method and the approximations behind it.

2.2. Density Functional Theory

DFT is based on the concept that the properties of any molecular system can be fully determined from its *electron density*, which represents the probability of finding any of the N electrons within the volume element dr. Since the electrons are indistinguishable, the probability of finding any electron at the $d\vec{r}$ position and ds spin is just N times the probability for one particular electron,

$$\rho(\vec{r}_1) = N \int \ldots \int |\Psi(\vec{r}_1, \vec{x}_2, \ldots, \vec{x}_N)|^2 ds_1 d\vec{x}_1 d\vec{x}_2 \ldots d\vec{x}_N \qquad [2.5]$$

where,

$$d\vec{x}_i = ds_i d\vec{r}_i \qquad [2.6]$$

Based on the properties of the electron density, in 1964 Hohenberg and Kohn[148] stated two theorems that represent the basis of the theoretical bedrock of DFT, as it is known nowadays.[149,150] They demonstrated that any observable of a stationary non-degenerate ground state could be calculated exactly from the electron density of its ground state. Furthermore, in order to obtain the exact energy of the system, the density that minimizes the energy of the ground state has to be found. The most interesting observable from the chemical point of view is the energy of the system, which can be expressed as:

$$E[\rho] = T[\rho] + V_{ee}[\rho] + V_{ne}[\rho] \qquad [2.7]$$

where T is the kinetic energy, V_{ee} is the electron-electron repulsion and V_{ne} is the nuclei-electron attraction. The T and V_{ee} terms are independent of the external potential and are collected into the universal *Hohenberg-Kohn functional* ($F_{HK}[\rho]$; Eq. 2.8). Regarding to the V_{ee} term, it can be split into the classical Coulomb part (J), which is exactly known, and the non-classical contribution (E_{ncl}), which is unknown.

$$F_{HK}[\rho] = T[\rho] + V_{ee}[\rho] = T[\rho] + J[\rho] + E_{ncl}[\rho] \qquad [2.8]$$

In 1965, Kohn and Sham[151] established a way to calculate F_{HK} by finding a reliable approach to the kinetic energy, T. Their basic idea was to obtain from a Slater determinant the exact kinetic energy of a non-interacting reference system, T_s, *being* $T_s < T$, with the same density as the real one (i.e. the interacting system). Then, $F_{HK}[\rho]$ is rewritten as:

$$F_{HK}[\rho] = T_s[\rho] + J[\rho] + E_{XC}[\rho] \qquad [2.9]$$

where E_{XC}, called *exchange-correlation energy*, is a new term that contains everything that is unknown, and is defined as:

$$E_{XC}[\rho] = (T[\rho] - T_s[\rho]) + E_{ncl}[\rho] = T_c[\rho] + E_{ncl}[\rho] \qquad [2.10]$$

It is important to realize that if the exact form of E_{XC} was known, the Kohn-Sham method would provide the exact energy. Thus, the approximation only comes into play when an explicit form of the unknown exchange-correlation functional is defined. Therefore, the difference between the DFT methods stems from this exchange-correlation expression.

2.2.1. Exchange-Correlation Energy

As stated before, a good exchange-correlation energy description is a fundamental aspect of DFT. The most common approximation is to consider the exchange and correlation contributions separately and then combine both into a single exchange-correlation expression:

$$E_{XC}[\rho] = E_X[\rho] + E_C[\rho] \qquad [2.11]$$

The E_X term considers that the motion of two electrons with parallel spins is correlated, while the motion of electrons with opposite spins remains uncorrelated. Otherwise, the E_C term covers the electrostatic repulsion between electrons. Different approximations to calculate the exchange-correlation energy exist, differing on the accuracy level and the computational cost.

The simplest way of representing the E_{XC} is the *Local Density Approximation* (LDA). It assumes that the E_{XC} only depends on the density locally treated as a uniform electron gas, where the electrons are moving on a positive background charge distribution. The LDA works well in systems where the density is maintained almost constant. Nevertheless, this total density is considered to be the sum of α and β spin densities, which is satisfied in closed-shell systems, but not in open-shell. The generalization of the LDA leads to the so-called *Local Spin Density Approximation* (LSDA), but these methods are not suitable for systems with week bonds or for making reliable thermochemical predictions. The next step, in order to improve LDA-based functionals, consists in introducing density gradients into the description of exchange-correlation effects. This represents the basis of the G*eneralized Gradient Approximation* (GGA), which is a semi-local correction since the exchange-correlation energy per unit volume still depends only on the density and on the density derivative at each point. Examples of GGA functionals are the B86 for exchange,[152] LYP for correlation[153] and PBE.[154]

Another step in the DFT development corresponds to the *meta-GGA functionals*.[155] These include an explicit dependence on the kinetic energy in the exchange term and/or the Laplacian of the density ($\nabla^2\rho(r)$). Among these functionals, there are the TPSS[156] and VSXC.[157]

An alternative strategy is to use the exact exchange energy provided by the HF method and rely on approximate functionals only for the part that HF does not cover, i.e. the electron correlation. This functionals are known as *hybrid functionals*, also *hyper-GGA*. The use of these hybrid methods can be justified by the so-called *Adiabatic Connection Formula* (ACF) for the exchange-correlation energy,

$$E_{XC}[\rho] = \int_0^1 E_{ncl}^{\lambda}\,[\rho]d\lambda \qquad [2.12]$$

where λ is the *coupling strength parameter* (with values between 0 and 1) and E_{ncl} is the non-classical contribution to the electron-electron interaction for different values of λ. At $\lambda = 0$, we are dealing with a non-interacting system and E_{ncl} is only composed of exchange, while at $\lambda = 1$ it corresponds to a fully interacting system and then, E_{ncl} contains both exchange and correlation terms. However, to solve the [2.12] equation for intermediate λ values some relation between the E_{ncl} and λ has to be considered. The simplest approximation is to assume a linear behavior between both, which leads to the *Half-and-Half* (HH) combination,[158] with a 50% of exact exchange and 50% of LDA exchange.

$$E_{XC}^{HH} = \frac{1}{2}E_X^{\lambda=0} + \frac{1}{2}E_X^{\lambda=1} \qquad [2.13]$$

One of the most widely employed variants of this combination is the BHandHLYP functional,[153,158,159] which has been shown to deliver particularly good results for radical systems.[160–162]

$$E_{XC}^{BHandHLYP} = \frac{1}{2}E_X^{exact} + \frac{1}{2}E_X^{LSDA} + \frac{1}{2}\Delta E_X^{B88} + E_C^{LYP} \qquad [2.14]$$

Further, there are other widely used methods based on adiabatic connections, such as the B3LYP[163,164] hybrid functional, which include empirical parameters to determine the amount of each different contribution.

$$E_{XC}^{B3LYP} = aE_X^{exact} + (1-a)E_X^{LSDA} + b\Delta E_X^{B88} + cE_C^{LYP} + (1-c)E_C^{VWN} \qquad [2.15]$$

Despite the wide use the B3LYP functional, this has significant pitfalls including a poor description of non-covalent interactions[165] (e.g. van der Waals) and the underestimation of energy barriers.[166] In this context, a new series of functionals namely the Minnesota "MXX" functionals of Truhlar et al.[165,167–170] and the *Grimme's dispersion correction* method (DFT-D),[171] appeared.

Another alternative are user-defined models which are obtained by first choosing gradient corrected exchange and correlation functionals from the list of available choices, and then specifying the mixing ratio of the various exchange and correlation energy terms. For the latter step, the *Gaussian* software employed in this thesis uses the general formula:

$$E_{XC} = P_2E_X^{exact} + P_1\left(P_4E_X^{Slater} + P_3dE_X^{non-local}\right) + P_6E_C^{local} + P_5dE_C^{non-local} \qquad [2.16]$$

The values for the P_x parameters are provided through the IOP switches IOP(3/76=xxxxxyyyyy), IOP(3/77=xxxxxyyyyy), and IOP(3/78=xxxxxyyyyy) with P_1 = xxxxx/10000 from IOP(3/76) etc. The use of this facility is illustrated for instance with the MPW1K type functionals by Truhlar and coworkers[172] developed to optimize reaction and activation energies of free radical reactions.

A further step towards chemical accuracy is the *fully non-local functionals* obtained by using the exact exchange and by evaluating a part of the electron correlation exactly. Examples of this are: the *Random Phase Approximation*

(RPA)[173–176] and the *Interaction Strength Interpolation* (ISI).[177] Although the computational cost scales rapidly with these methods some advances begin to appear, such as the so-called double hybrid functionals, which combine the correlation of density functionals and MP2-like corrections.[178]

New density functionals continue to appear with the aim of improving the description of excited states and weak interactions. However, so far any of them has been shown to stand out to the others. Thus, the selection of the functional will depend on the chemical system under study, the level of accuracy required, e.g. including dispersion if the system involves many non-covalent interactions, and the computational cost associated. Hence, the user should be able to carefully choose the most appropriated functional on the basis of experimental data and/or high-level post-HF theoretical methods.

2.2.2. Description of Open-shell Systems

In this thesis, we have investigated the reaction mechanism of different oxidation processes involving transition metal catalysts. These metals have d-orbitals that are usually very close in energy, which enables several spin states depending on the oxidation state of the metal, its coordinated ligands and its geometry. The accurate description of spin-state splittings in transition-metal complexes is very sensitive to the employed exchange-correlation functional, and in particular, to the exchange part. In 2001, Reiher and co-workers[179] analyzed the effect of the amount of exact Hartree-Fock exchange in a number of exchange-correlation functionals. They showed that high-spin states are systematically favored in HF-based theories because Fermi correlation is included in the exact exchange, whereas Coulomb correlation is not. Thus, although there is no clear evidence of which functional performs best, the rule of thumb is that pure functionals, e.g. BP86, tend to overestimate the stability of low-spin states, while hybrid ones, e.g. B3LYP, favor high-spin states.[180] Consequently, computational studies should include an attempt to benchmark the chosen method by comparing it to experimental data or an accurate *ab initio* method such as CCSD(T). The choice of functionals and basis sets used in this thesis is discussed in the next section.

2.3. Scope of Application

This section is devoted to explain how all the computational methodologies above described have been applied to the current dissertation. First, the exchange-correlation functionals and basis sets employed for each of the investigated projects are discussed. Then, the potential energy surface concept is introduced, as it provides the energetic landscape of the studied reactions. Finally, the general scheme employed in this thesis to calculate the Gibbs energies is presented.[181–183]

2.3.1. Exchange-Correlation Functionals Employed

In the organometallic chemistry field, several benchmark studies have been compiled in the literature covering the performance of different density functionals for their application in chemical systems. For the topics included in this Ph.D. thesis, the most utilized functionals are hybrid GGA and meta-GGA. Particularly, in discrete systems we used B3LYP in the treatment of water oxidation reactions and BHandHLYP and MPWB1K[184] in the C−H oxidation reactions, whereas in periodic systems the GGA functional *Perdew−Burke−Ernzenhof* (PBE) was employed.

In the case of the water oxidation reaction, DFT(B3LYP) calculations were complemented by single point calculations with the M06 functional to assess the influence of dispersion forces on the energy barriers. As regards to the C−H oxidation of alkanes and alkenes by means of a copper-trispyrazolylborate catalyst, the BHandHLYP functional was used. The choice of this functional was based on a previous work reported by Sodupe and Rodriguez-Santiago,[160,185] where a series of Cu−H_2O complexes were studied with several DFT functionals and benchmarked with CCSD(T) calculations. Therein, the functionals that compared better to CCSD(T) were those with a large percentage of exact exchange, such as the BHandHLYP functional and its improved version known as MPWB1K[186,187]. Moreover, we also selected the BHandHLYP functional because it was shown in previous works[160–162] to deliver particularly good results in describing radical systems.

For the mechanistic study on the C=C oxidation reaction, calculations were performed employing the MPWB1K functional. This functional developed by Zhao and Truhlar,[165,184] has a 44% of exact exchange and it includes dispersion corrections, which provides very good results in the modeling of open-shell hydrogen-transfer reactions and the description of non-covalent weak interactions.

On the other hand, the PBE functional was employed to model the water oxidation reaction catalyzed by the IrO_2 surface, based on the good results obtained in previous works involving metal oxides.[188,189]

2.3.2. Basis Sets

In order to overcome the problem of exactly solve the Schrödinger equation for many electron systems, in 1930 Hartree Fock proposed the *Self-Consistent Field* (SCF) method.[190,191] It consists in an iterative method that involves selecting an approximate Hamiltonian, solving the Schrödinger equation to obtain a more accurate set of orbitals, and then solving the Schrödinger equation again until results converge. However, the SCF calculations were not to become truly operative until the introduction of the *Linear Combination of Atomic Orbitals* (LCAO) in 1951 by Roothaan and Hall.[192] This approximation requires the definition of a set of functions, ϕ_μ, known as atomic basis set, to expand the spatial part of the spin orbitals, φ_i, according to:

$$\varphi_i = \sum_\mu c_{\mu i}\phi_\mu \qquad [2.17]$$

where $c_{\mu i}$ are the linear coefficients of the expansion. Unfortunately, this expression is exact only with an infinite number of functions and in practice it has to be approximated by using a finite basis set. The choice of this basis is crucial for a good description of the *atomic orbitals* (AO). In a very general sense, basis sets can be divided into two big groups: the *orbital-like functions* and the *plane waves*.

2.3.2.1. Orbital-like Functions

Molecular systems are usually modeled by orbital-like functions, i.e.

functions that are centered in nuclear atoms and whose shape is similar to the orbital functions obtained for one-electron atoms. Particularly, the ones concerning this Ph.D. thesis are *Gaussian Type Functions* (GTFs), which have this general form:

$$\phi_{\alpha,n,l,m}(r,\theta,\varphi) = N x^{l_x} y^{l_y} z^{l_z} e^{-\alpha r^2} \qquad [2.18]$$

where N is a normalization constant, $l_x + l_y + l_z$ the sum that determines the type of orbital, α the pre-exponent and r the distance between the nuclei and electron.

In fact, a set of known functions is not an approximation if the basis set is complete. However, a complete basis set means that an infinite number of functions must be considered, which is impossible in actual calculations. Thus, the most important issue is the number of functions to be used. One way to increase the minimum basis sets is by doubling or tripling all the basis functions, producing a *double* or *triple zeta* type basis. In this functions only the s- and p- functions of each atom are considered although in most cases, higher angular momentum functions are also important. These are denoted *polarization functions*, which alter the orbital shape, making them more flexible and more suitable for the description of chemical bonds. Furthermore, *diffuse functions* can be also incorporated, allowing larger electron delocalization over space, which can be critical for anions.

Systems involving transition metals from the second and the third row of the periodic table have a large number of core electrons and present relativistic effects. These two problems may be solved by *pseudopotentials* or *Effective Core Potentials* (ECP), which replace the electron density from the inner electrons with a potential core, and treat only the valence electrons explicitly. Several pseudopotentials have been developed and used especially in transition metal computational chemistry due to their large electron population. Two of the most highlighted in the literature and employed in this Ph.D. are: Los Alamos National Laboratory (LANL)[193] and the Stuttgart-Dresden (SDD) pseudopotentials. [194,195]

2.3.2.2. Plane Wave Functions

Solid materials are usually represented by a unit cell, which is repeated periodically in space by lattice vectors a_1, a_2 and a_3. The solutions of the Schrödinger equation for these periodic systems are spatially extended functions, commonly known as *plane waves* that satisfy the *Bloch's theorem*:[196]

$$\psi_i(r) = e^{(ik.r)}u_i(r) \qquad [2.19]$$

where r is the position vector, k the wave vector and $u_i(r)$ the lattice periodic function. This periodic function $u_i(r)$ can also be expressed as a sum of plane waves whose wave vectors, G, are reciprocal lattice vectors of the crystal:

$$u_i(r) = \sum_G c_{i,G} e^{[iG.r]} \qquad [2.20]$$

Thus, the electronic wave function results in a total plane wave expansion defined as:

$$\psi_i(r) = \sum_G c_{i,k+G} e^{[i(k+G)r]} \qquad [2.21]$$

where $c_{i,k+G}$ are the expansion coefficients for the plane waves.

Bloch's theorem uses the periodicity of the crystal to reduce the infinite number of one-electron wavefunctions to simply the number of electrons in the unit cell of the crystal. Thus, by using this theorem, the problem of the infinite number of electrons is mapped onto the problem of expressing the wavefunction in terms of an infinite number of reciprocal space vectors within the *Brillouin zone*[1] of the periodic cell, k.

According to the expression [2.21], a single point in the *k-space* involves a summation over an infinite number of possible values of G. However, each coefficient $c_{i,k+G}$ has a kinetic energy that is also a solution of the Schrödinger equation, Eq [2.22]. Therefore, as it is reasonable to expect that solutions with lower energies have a more important role than those with a high kinetic energy, only solutions below a given energy cutoff, E_{cut}, are considered.

---

[1] Brillouin Zone is the equivalent of a unit cell in reciprocal space.

$$E = \frac{\hbar^2}{2m}|k+G|^2 \quad \rightarrow \quad E_{cut} = \frac{\hbar^2}{2m}G_{cut}^2 \qquad [2.22]$$

Then, the infinite sum in equation 2.21 is reduced to:

$$\psi_k(r) = \sum_{|k+G|<G_{cut}} c_{k+G}\, e^{[i(k+G)r]} \qquad [2.23]$$

However, the problem arises with core electrons, since large energy cutoffs must be used to include plane waves that oscillate on a short length scale. To handle this issue, pseudopotentials are also employed in periodic systems. In the present work, the Projector Augmented Wave (PAW) method introduced by Blöchl[197] and adapted for plane-wave calculations by Kresse and Joubert,[198] has been used to describe the core electrons.

2.3.3. Potential Energy Surface

The *potential energy surface* (PES) represents the energy of a chemical system as a function of its nuclear coordinates. There are two types of PES: adiabatic and diabatic. Adiabatic surfaces are defined within the Born-Oppenheimer approximation by the energy (eigenvalue) of a given solution to the electronic Schrödinger equation at each geometry. Such solutions are obtained by using the full electronic Hamiltonian, that is, including kinetic energy, Coulomb, scalar relativistic and spin-orbit terms. On the other hand, diabatic surfaces can be defined as generated from the eigenvalues of the Schrödinger equation solved using a Hamiltonian from which one or more terms have been omitted, such a the spin-orbit coupling. In the present case, adiabatic surfaces have been considered.

Hence, a complete analysis of the PES reveals the overall energy landscape with respect to the atomic positions (Figure 2.1). Unfortunately, its entire construction is only feasible for small systems, since it has *3N−6* degrees of freedom in non-linear systems, where *N* is the number of atoms.

From the chemical point of view the most interesting geometries correspond to stationary points of the PES: *local minima* and *saddle points*. In the former, the eigenvalues of the Hessian matrix, which collects the second derivatives of the energy, are all positive. Local minima correspond to the reactants, intermediates and products of a chemical reaction. In contrast, saddle points have one negative eigenvalue in the Hessian matrix, which means that they are an energy minimum in all directions except one, in which they are maximum. The latter direction corresponds to the energy pathway connecting reactants to products. These points are known as transition states and their energy determines the energy barrier and rate constant of the reaction.

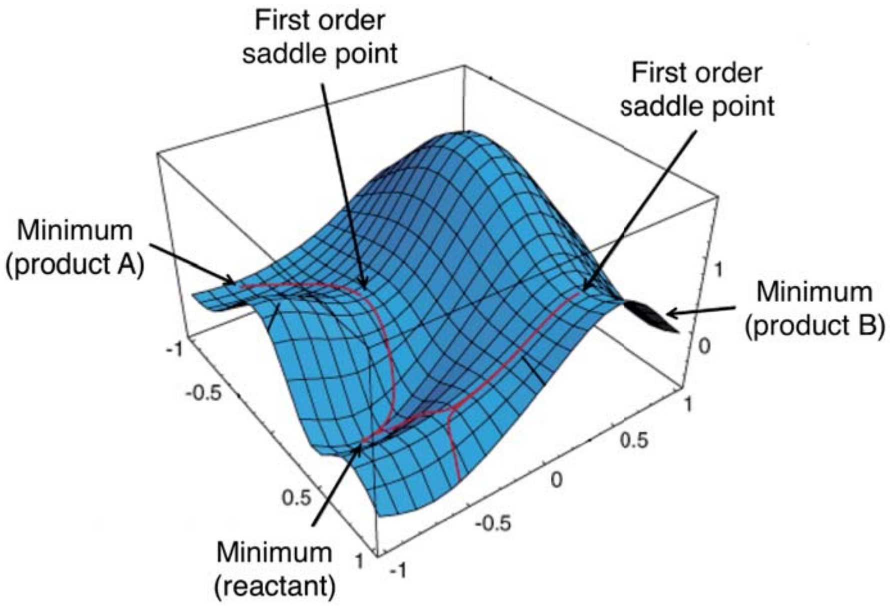

Figure 2.1: Example of a 3D-representation of an arbitrary PES.

Finding stationary points in a PES requires the choice of an appropriate methodology, which includes the selection of the level of theory (e.g. Molecular Mechanics, Quantum Mechanics), the method (e.g. Hartree-Fock, DFT), the basis set (e.g. double-zeta, pseudopotentials, polarization functions) and the solvation model (e.g. continuum model, explicit solvent molecules). In the particular case of transition states, their location is frequently not trivial and in addition to require an appropriate methodology, "chemical intuition" is also needed. One way to verify that these first-order saddle points connect the corresponding reaction minima is by using the Intrinsic Reaction Coordinate (IRC) method. This method consists in following the line of steepest decent towards either side of the transition state. After their full optimization, the nature of these stationary points is further assessed by computing the first (gradient) and second (hessian) derivatives of the energy with respect the nuclear coordinates, as above-mentioned.

2.3.3.1. Minimum Energy Crossing Points

Given that oxidation reactions usually involve O_2 or oxo species, it is common to find different spin states for the intermediate species involved along the reaction path.

These reactions are said to be non-adiabatic in the sense that they occur in more than one PES. Thus, the spin change requires the system to “hop” from the PES associated to the initial spin state onto the one corresponding to the product state. Briefly, this can be understood as the motion of the atoms brings the system into a region where the two surface cross, or are close enough, that the corresponding spin-orbit coupling enables the “hop” from one surface to the other (Figure 2.2).

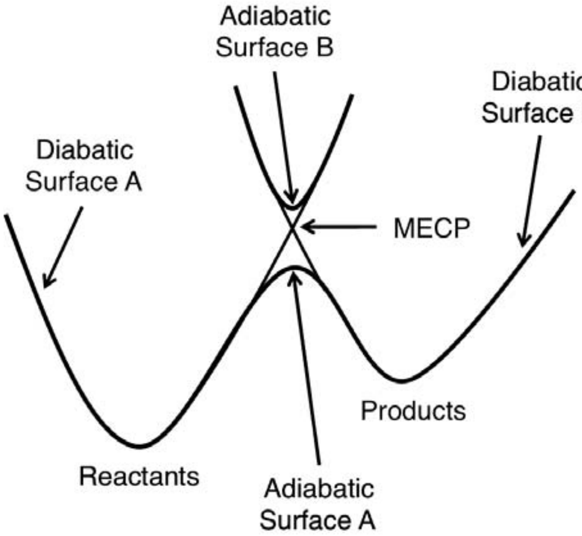

Figure 2.2: Schematic diabatic and adiabatic potential energy surfaces for a Spin-forbidden reaction.

The probability of crossing from one spin state to the other decreases with the energy of the Minimum Energy Crossing Point (MECP), but increases with the spin-orbit coupling of the system, which is strong with many transition metals. In the adiabatic description, the MECP corresponds to the crossing point between two PES, in which the structure of the system has exactly the same potential energy for both spin states.

In the present thesis, MECPs are located by using a program developed by Harvey *et al.*[199] based on the steepest descent method. More specifically, it consists in combining the energies, E_i, of the two PESs and their corresponding energy gradients ($\delta E_i/\delta q$) with respect to the nuclear coordinates q, to yield two effective gradients, f and g, Eq. [2.24] and [2.25]. These vectors are orthogonal to each other and go to zero at the MECP, where the energy gradients on the two surfaces are parallel. The criteria employed to test the convergence of the MECP are the same used in Gaussian a part from a threshold of 0.000050 for the ΔE.

$$f = (E_1 - E_2)\left[\left(\frac{\delta E_1}{\delta q}\right) - \left(\frac{\delta E_2}{\delta q}\right)\right] = (E_1 - E_2)x_1 \qquad [2.24]$$

$$g = \left(\frac{\delta E_1}{\delta q}\right) - \frac{x_1}{|x_1|}\left[\left(\frac{\delta E_1}{\delta q}\right)\left(\frac{x_1}{|x_1|}\right)\right] \qquad [2.25]$$

2.3.4. Solvation Models

Most of the chemical reactions in homogeneous catalysis are performed in the presence of a solvent. There are three different models for evaluating the solvent effect, namely explicit, implicit and hybrid explicit-implicit models.

The explicit solvent model consists in including only explicit solvent molecules in the calculation. This can be done through a cluster solvent model or a full description of the solvent. In the former, only a few solvent molecules are taken into account, whereas in the latter a large number of solvent molecules are included surrounding the solute. The full description of the solvent can be carried out by *molecular dynamics* (MD) simulations, which do concern the time evolution of atoms under periodic boundary conditions (PBC). MD invokes classical Newton's equations motion in which the magnitude and direction of motion are ruled by forces that are computed from force fields (classical MD) or quantum mechanics methods (*ab initio* MD). The major advantage of classical MD is its ability to deal with environmental effects, such as solvent and temperature, and to tackle large macromolecules in realistic surrounding due to its low cost. However, the main drawbacks arise in the non-proper description of transition metals with force fields and the bond-breaking situations. To overcome these issues *ab* *initio* MD simulations[200] can be used, although it entails expensive computational demands.

A more affordable strategy is to consider the solvent implicitly as a continuum medium. Among this type of methods, there is the *self-consistent reaction field* (SCRF),[201] which considers the solvent as a uniform polarizable medium with a dielectric constant ε, with the solute placed in a void cavity. In particular, the models that have been used in the present thesis are the *polarizable continuum model* (PCM)[202] and the *solvent model density* (SMD).[203] These two models define the cavity for the solute as the union of a series of interlocking spheres centered on the atoms and differ in that the latter includes the radii and non-electrostatic terms suggested by Truhlar and coworkers.

And the last approach consists in considering some explicit solvent molecules in the first coordination sphere and the rest with a continuum representation. This hybrid approach is commonly referred as discrete-continuum model and it is most often used when the solvent is involved in the reaction. This model, in which a reduced number of explicit solvent molecules are considered, has been successfully applied in computational studies of the organometallic reactivity.[204–206]

Regarding heterogeneous catalysis, implicit solvation models for plane wave DFT codes are the most common ones. These were initiated in 2003 by Fattebert and Gygi[207] and later extended by Marzari *et al.* [208] to include a model for cavitation and dispersion. Nowadays, these models provide an accurate description for understanding solute/solvent interfaces at a reasonable computational cost.

2.3.5. Gibbs Energies in Solution

The Gibbs energies in solution can be expressed as the sum of the $(G - E)_g$ term, which includes the zero-point energy (ZPE), and the thermal and entropy contributions, to the energy in solution (E_{sol}), obtained by a single point calculations on the gas-phase optimized geometries.

$$G_{sol} = (G - E)_g + E_{sol} \qquad [2.26]$$

Although this can be a rough approximation, normally provides good results except in the case of dissociative and associative processes. This is because in gas phase the translational and rotational contributions to the entropy are larger than those in solution phase. In this last case the molecules are surrounded by the solvent and consequently, they cannot freely move and rotate as they do in gas phase. Hence, the computational study of dissociative process in condensed phase results to be more favorable than what it really is, whereas associative processes turn out to be less favorable. To handle this issue, different approaches have been developed in the last decades. For example, some authors have proposed to only consider the vibrational contribution to the entropy,[209,210] but if the previous approximation overestimates the entropy, this one underestimates it. Therefore, another approximation is the one proposed by Ziegler et al. based on the Wertz model.[211] With this model, G_{sol} is expressed as:

$$G_{sol} = E_{sol} + ZPE + H_{vib} + 6k_B T - TS_{mod} \qquad [2.27]$$

where H_{vib} is the vibrational enthalpy and S_{mod} is the entropy calculated using the Wertz's approximation for the entropy fit to the experimental solvation entropy of small molecules,

$$S_{mod} = S_{elec} + S_{vib} + 0.54(S_{trans} + S_{rot}) + 0.24 \qquad [2.28]$$

where S_{elec}, S_{vib}, S_{trans}, and S_{rot} are the electronic, vibrational, translational and rotational contributions to the entropy, respectively.

"All successful people men or women are big dreamers. They imagine what their future could be, ideal in every respect, and then work everyday toward their distant vision, that goal or purpose"

Brian Tracye

3

Objectives

The main objective of this dissertation is to apply computational methods to the study of metal-catalyzed oxidation reactions in order to gain a mechanistic view of these important processes. More specifically, we have focused on the mechanistic study of some of the most relevant oxidation reactions: the water oxidation, the oxygenation of C=C bonds and the oxidation of C−H bonds in inert hydrocarbons.

Water Oxidation Reaction

Extensive research has been directed toward elucidating and understanding the fundamental steps involved in the water oxidation reaction. However, the mechanistic complexity and the high oxidation potential required to oxidize water make the rational design of novel catalysts a challenging task. The mechanism of this reaction has been investigated in both homogeneous and heterogeneous systems. The main goals of these studies are:

- Understanding the effect of the metal-ligands.
- Evaluating the pH effect on the nature of the catalytically active species.
- Comparing the water nucleophilic attack and the direct coupling mechanisms.
- Studying the possibility of combining homogeneous and heterogeneous catalysts, in order to benefit from a mixed approach.

Oxygenation of C=C bonds

The oxidation of C=C bonds is usually a highly exothermic process, in which the detection of intermediate species able to provide some hint about the reaction mechanism is very difficult. Hence, in order to shed light into these processes, we carried out a theoretical study with the following objectives:

- Determining the oxygenation mechanism of C=C bonds with Rh- and Ir-based complexes using molecular oxygen.
- Providing a plausible explanation for the different experimental products obtained with two similar complexes.

- Analyzing the influence of the metal and the ligand on the outcome of the reaction.

Oxidation of C-H bonds

Most of the reported catalytic systems for the hydroxylation of inert C-H bonds require strong reaction conditions including acidic medium, which entails mixtures of different oxidation products. In 2011, Pedro Pérez *et al.* reported the acid-free oxidation of benzene with H_2O_2 in the presence of Cu-based catalysts under mild conditions. In order to get a deeper understanding of this catalytic system and the operating reaction mechanism, a theoretical study in collaboration with the group of Prof. Pedro J. Pérez was carried out, with the following common objectives:

- Determining the catalytic Cu active species in these oxidation processes.
- Analyzing the hydroxylation reaction of benzene by means of an electrophilic aromatic substitution and rebound mechanisms.
- Studying the effect of *para*-substituents in the benzene ring on the reactivity.
- Providing a detailed picture of the cyclohexane oxidation reaction with the Cu catalyst, in order to explain the product mixtures observed experimentally.
- Rationalize the experimental data.

"Start by doing what's necessary: then do what's possible: and suddenly you are doing the impossible."

Francis of Assisi

4

Bernhard's Water Oxidation Catalyst

In this chapter a theoretical study on the water oxidation reaction catalyzed by the Ir(III) complex $[Ir(H_2O)_2(ppy)_2]^+$ (ppy = *o*-phenylpyridine) is presented. Three possible protonation states of the Ir(V) active species, $[Ir(O)(X)(ppy)_2]^n$, with X = OH_2 (n = +1), OH^-, (n = 0) or O_2 (n=-1), have been considered for the O−O bond formation. The reactivity of each of these species has been investigated and the dependence of the energy barriers on the nature of the ligand X analyzed. The results derived from this work show the detrimental influence of the X ligand on the critical O−O bond formation step.[212]

4.1. Introduction

In the last years, important developments in the field of homogeneous catalysis for water oxidation have been carried out, both in the design of molecular catalysts and in the mechanistic reaction insight.[213,214]

A keen interest in molecular systems arose after Meyer and coworkers in the eighties developed a dimeric Ru(II) catalyst, called the blue dimer (Scheme 4.1a).[215] In the belief that two metal centers were essential to ensure the efficient water oxidation reaction a variety bimetallic systems were developed.[46–50] However, in the last few years, a new generation of mononuclear water oxidation catalysts has emerged, which are much more easily characterized and modeled than the polynuclear ones.

Especially interesting are mononuclear catalysts based on nature-inspired, abundant and inexpensive metals such as, Mn[55], Co[70] and Fe[67–69] (Scheme 4.1). Unfortunately, these systems usually suffer from little stability and activity drops off after short time of catalysis. On the other hand, catalysts containing precious metals, such as Ru[45,56–58] and Ir[61–63] (Scheme 4.1) are highly active and are often the most robust ones.

In the particular case of ruthenium complexes, a significant progress has been made by Meyer's[56] and Thummel's[57] groups, which corroborate that single Ru site constitutes a family of robust catalysts. Otherwise, with regard to Ir-based catalysts, Bernhard and co-workers[61] reported the first mononuclear iridium water oxidation catalyst based on two previous bimetallic catalysts reported by Grätzel *et al.*[48] and Thummel and Zong.[57] Since then, several groups focused on mononuclear Ir-based catalysts and have been working to improve the catalytic activity reported by Bernhard *et al.* It is worth mentioning the work carried out by Crabtree and co-workers,[44,62] with a wide variety of Cp* iridium complexes, and the two highly active Ir(III) catalysts by Macchioni *et al.* [63]

Scheme 4.1: Examples of homogeneous water oxidation catalysts.

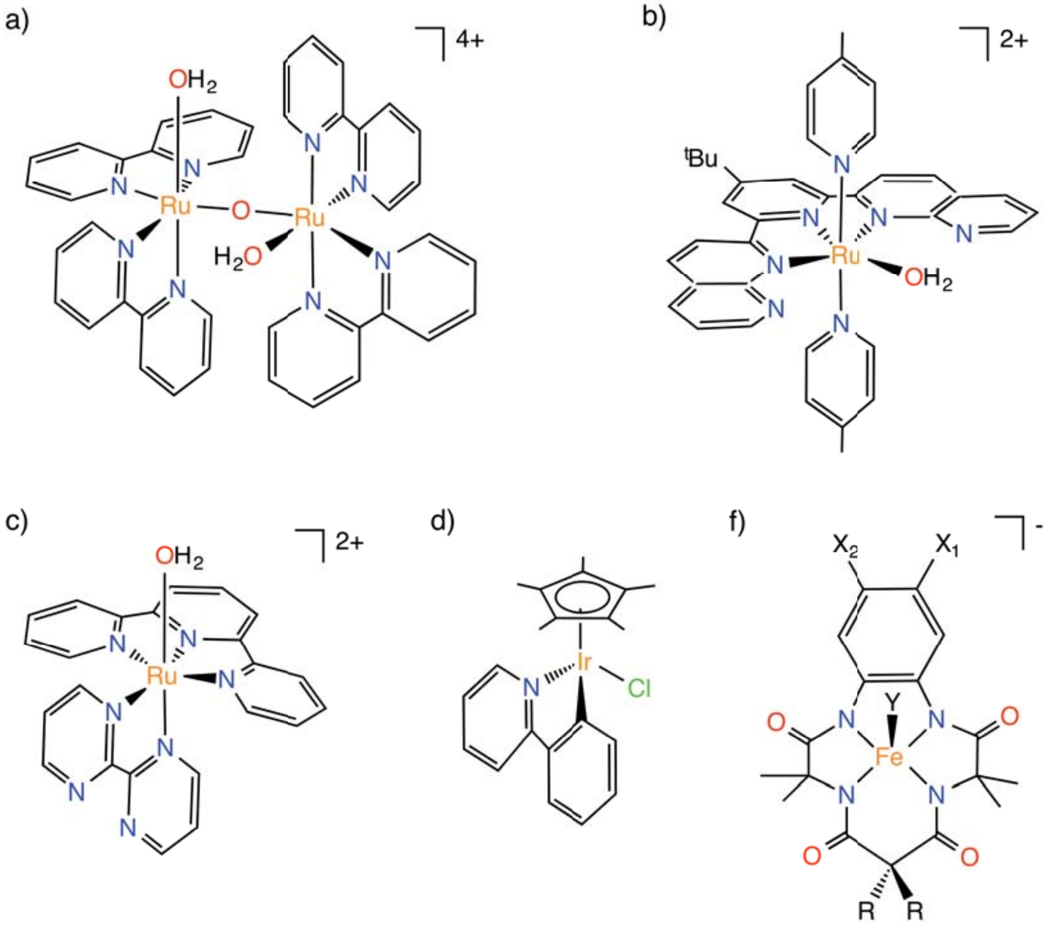

Although many promising synthetic molecular water oxidation catalysts have been reported, much work needs to be performed in order to reach large-scale applications. Current efforts are focused on enhancing both the catalytic efficiency and robustness of these systems and on building them with less toxic, more abundant and thus cheaper metals.

4.1.1. Bernhard's Catalyst

Bernhard's catalyst precursor (Scheme 4.2) consists in a cationic bis-aqua Ir(III) complex, $[Ir(OH_2)_2(phpy)_2]^+$ (phpy = phenylpyridine) synthetized by treating a chloride-bridged Ir(III) dimer, containing cyclometalated phpy ligands, with silver triflate. The catalyst is robust under typical reaction conditions, water soluble on a wide pH range and easily tunable by changing the nature of the R_n substituents with various electron withdrawing and/or electron-donating groups.

Scheme 4.2: Bernhard's Catalyst.

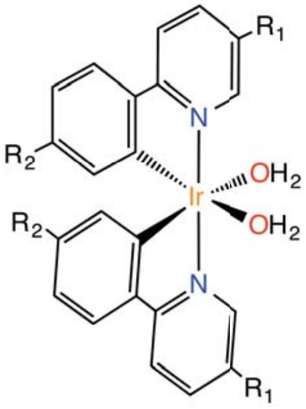

In the present computational study we chose the Bernhard's catalyst with the aim of rationalizing its acid/base properties in the water oxidation reaction. First of all, it is important to be aware of what reaction mechanism is involved in this process. A plausible catalytic cycle for this system, which has been already postulated for other single metal catalysts,[62,74,75] is the one represented in Figure 4.1.

The reaction starts with the oxidation of the Ir(III)−OH_2 complex by the sacrificial oxidant cerium(IV) ammonium nitrate (CAN), leading to the formation of the Ir(V)=O moiety, which has been already proposed in previous works as the active species in the formation of the O−O bond.[216–218] In fact, the need for a highly electrophilic metal-oxo fragment may be ascribed to the poor nucleophilic character of H_2O. Finally, the catalytic cycle is closed by further oxidation of the resulting peroxo intermediate giving rise to the formation of molecular oxygen and the recovery of the catalyst. In this work, we focused on the O−O bond formation step, since it corresponds to the rate-determining step for many Ir-based water oxidation catalysts.[217,219,220]

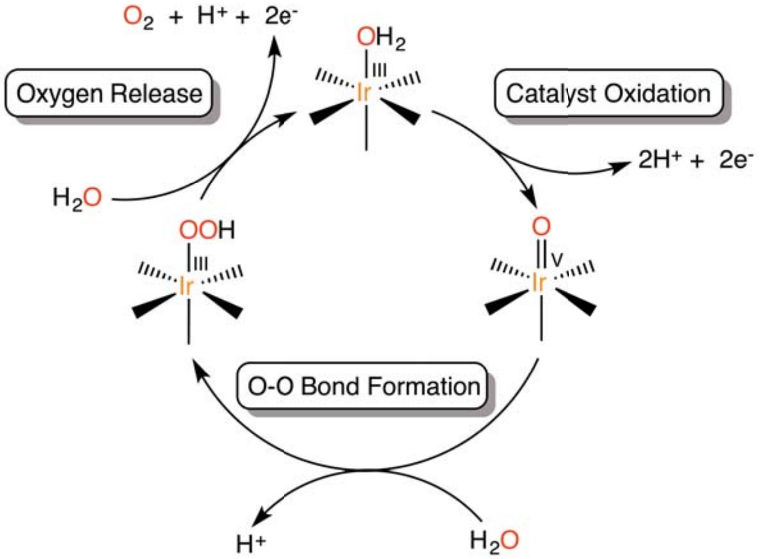
O_2 + H^+ + $2e^-$
Oxygen Release
OH_2
III
Ir
Catalyst Oxidation
$2H^+$ + $2e^-$
H_2O
OOH
III
Ir
O
V
Ir
O-O Bond Formation
H^+
H_2O

Figure 4.1: Catalytic cycle postulated for water oxidation reaction in the presence of a mononuclear iridium catalyst.

The O−O bond formation step can be described as an acid/base reaction,[74,221] where the Ir(V)=O moiety acts as a Lewis acid by accepting two electrons from a water molecule. In addition, a Brønsted base can also take part in the mechanism by accepting the proton released by water. In the absence of an external base,[75,81] the proton acceptor, namely X, can be either the Ir(V)=O moiety[73] or an ancillary ligand of the catalyst itself[82,83] (Scheme 4.3). The theoretical study reported herein shed light on the dramatic effect caused by the nature of the proton acceptor on the activity of the Bernhard's catalyst.

Scheme 4.3: Acid/base mechanisms for O−O bond formation, with the proton transferred to either the Ir(V)=O or the X ancillary ligand. C^N = phpy ligand.

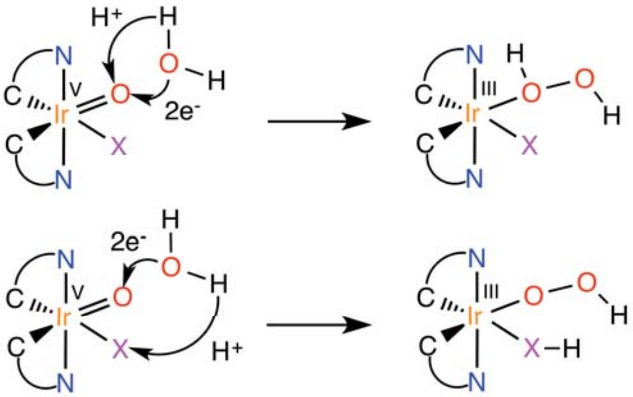
H^+
H
O
H
N
V
C
Ir
O
$2e^-$
C
X
N
N
H
III
C
Ir
O
O
H
C
X
N
H
$2e^-$
O
H
N
V
C
Ir
O
C
X
H^+
N
N
III
C
Ir
O
O
H
C
X−H
N

The postulated active species for the Bernhard's catalyst is the Ir(V) $[Ir(O)(X)(phpy)_2]^n$ complex, with X = OH_2 (n = +1), OH^- (n = 0) or O^{2-} (n = -1) depending on the pH of the media (Scheme 4.4).[222,223] Interestingly, all these complexes contain the Ir(V)=O moiety able to promote the formation of the O−O bond by the nucleophilic attack of water. Nonetheless, the different Lewis acidity of this moiety and Brønsted basicity of the X ligand in each species may affect the formation of the O−O bond. Thus, these three protonation states have been investigated as potential active species with the aim of rationalizing the interplay between Lewis acidity and Brønsted basicity in this catalytic system.[212]

Scheme 4.4: Protonation states of the Ir(V)=O active species for the Bernhard's catalyst.

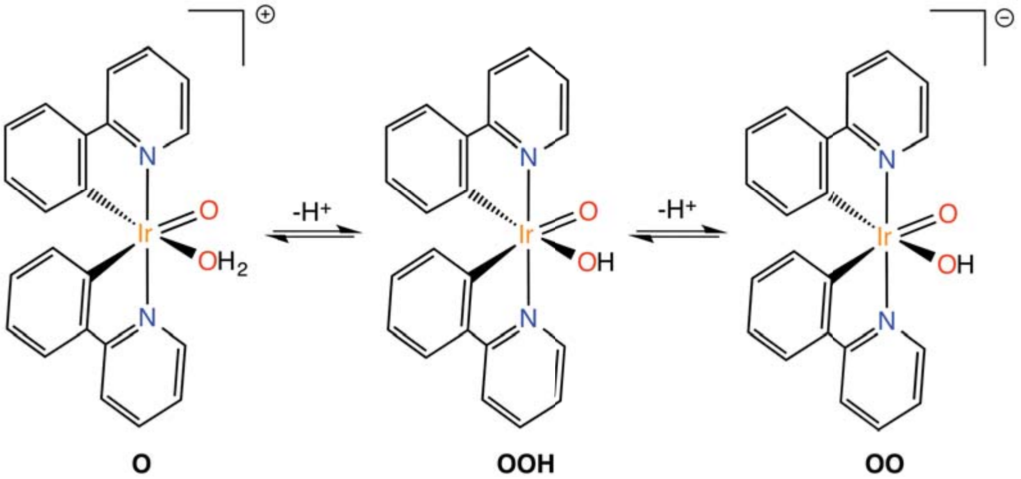

4.2. Computational Details

All the theoretical calculations in this study were carried out at the DFT level by means of B3LYP hybrid functional as implemented in the Gaussian09 software package.[224] Geometry optimizations were performed using the 6-31G(d,p) basis set for C, N, O and H atoms and the Stuttgart-Drensen scalar relativistic ECP with its associated double-ζ basis set for Ir. For this atom, f-polarization functions were also added (exp = 0.950). Geometries of all the reactants, intermediates and transition states were fully optimized without any symmetry or geometry constrain. Moreover, the reaction pathways were further checked by means of IRC calculations, in order to confirm that each transition state was connected to its corresponding reactant and product. The nature of these stationary points, which are all in a closed-shell singlet state, was characterized by a vibrational analysis performed within the harmonic approximation. Hence, transition states were identified by the presence of one imaginary frequency, whereas the minima by a full set of real frequencies. These frequency calculations were also used to determine the zero-point, thermal and entropy contributions to the energy, which were computed at a pressure of 1354 atm to simulate the entropy change in the condensed real phase.[225,226] These contributions were calculated as the difference between the gas phase potential and Gibbs energies, $(G\!-\!E)_g$.

Solvent effects (i.e. water) were introduced by single point CPCM[202] calculations on the gas phase optimized geometries, using the same basis set and pseudopotential for Ir but the larger 6-311+G(d,p) basis set for all the other atoms, E_{sol}. Thus, energies discussed in this study correspond to Gibbs energies in water, G_{sol}, obtained by employing the following formula:

$$G_{sol} = (G - E)_g + E_{sol} \qquad [4.1]$$

Furthermore, to assess the influence of dispersion forces, which may play a significant role in this reaction, we also performed single-point calculations by using the M06 functional on the B3LYP-optimized geometries with the large basis set.

4.3. Results

4.3.1. O–O Bond Formation Mechanism

In acidic conditions, the reaction may be promoted by the cationic $[Ir(O)(H_2O)(phpy)_2]^+$ species (Scheme 4.4). However, this species is not stable because, after its optimization, the water molecule decoordinates from the metal making a hydrogen-bond with the oxo ligand, d(O···H) = 1.962 Å, **O-1**. It results in a five-coordinated trigonal bipyramid complex, in which the oxo is in the equatorial plane with an Ir–O bond distance of 1.788 Å.

The energy profile showed in Figure 4.2 starts with the reactant **O**, which results from the reoptimization of the **O-1** intermediate without the water molecule. Even so, all the energies are referenced to the more realistic **O-1** intermediate, since water represents the solvent, but also the reactant. In the transition state **O-TS** (Figure 4.4), water makes an O–O bond with the oxo ligand, d(O···O) = 2.010 Å, which induces the Ir–O bond elongation to 1.969 Å. At the same time, a proton is transferred from the water molecule to the oxo ligand yielding to the **O-2** product that corresponds to a hydrogen peroxide bounded to the metal in a η¹-fashion, d(Ir–O) = 2.371 Å. This five-coordinated product is now far from an ideal trigonal bibyramid geometry and is more in accordance with an unsaturated octahedral complex.

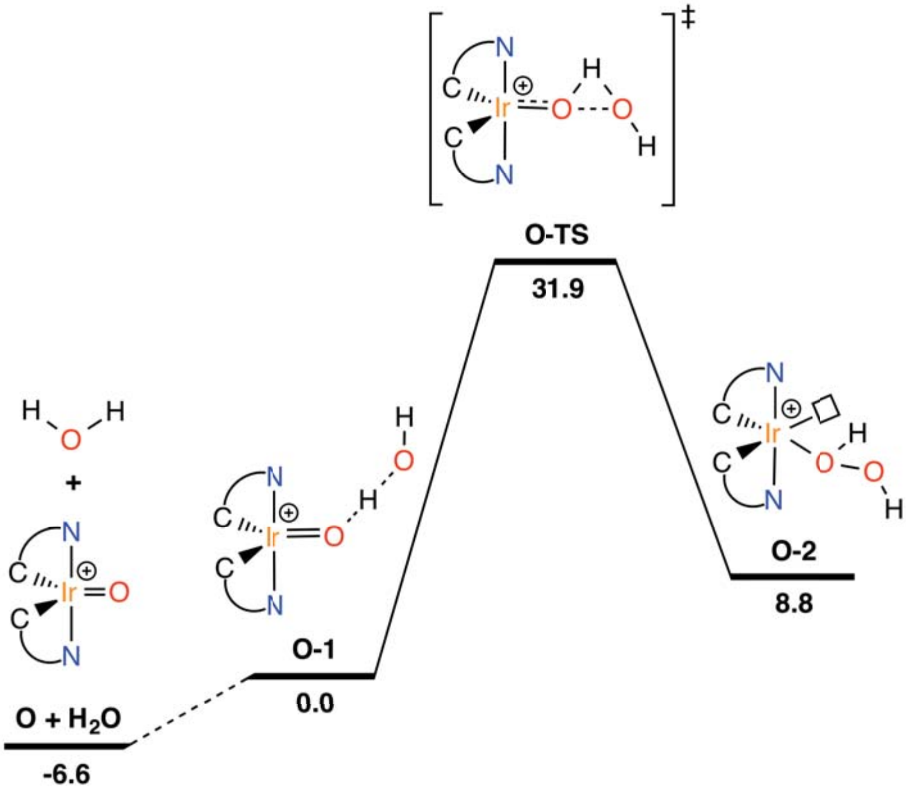

Figure 4.2: Gibbs energy profile, in kcal·mol⁻¹, for the formation of the O–O bond with the cationic **O** active species. The vacant site is represented as □ and C^N = phpy ligand.

According to the Gibbs energy profile represented in Figure 4.2, the generation of the vacant site may explain the unfavorable character of the reaction, which is endoergic, ΔG_{sol} = 8.8 kcal·mol⁻¹ and involves a high energy barrier, $\Delta G^{\ddagger}_{sol}$ = 31.9 kcal·mol⁻¹. Based on these results, an alternative pathway with one extra explicit water molecule, which may facilitate the reaction by capping the open vacant site, was also explored (Figure 4.3).

As in the case above-mentioned, the oxo ligand is also the responsible of making the O–O bond and accepting the proton released from water, even though in **O-TS'** (Figure 4.4) a second water molecule is bound to the metal center in a *cis* position. The product obtained, **O-2'**, is an octahedral η^1-H_2O_2 complex similar to the previous **O-2**, but with the vacant site occupied by an aqua ligand, d(Ir–OH_2) = 2.368 Å.

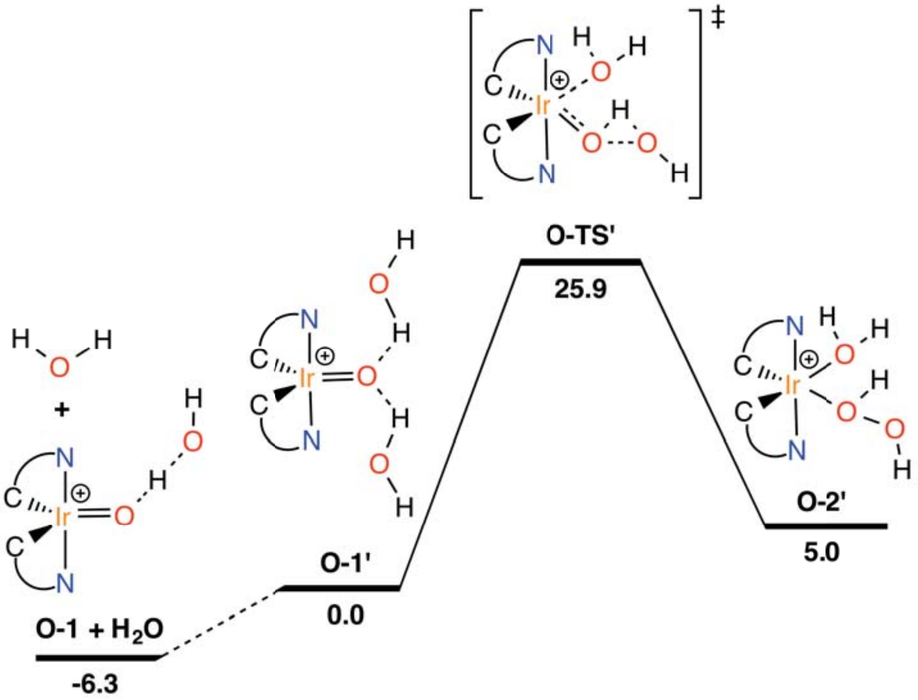

Figure 4.3: Gibbs energy profile, in kcal·mol^{-1}, for the O–O bond formation with the cationic **O-1** active species and one extra explicit water molecule.

The computed reaction profile shown in Figure 4.3 indicates that the participation of an extra water molecule makes the process less endoergic, ΔG_{sol}= 5.0 kcal·mol^{-1}, and also more feasible from the kinetic point of view, $\Delta G^{\ddagger}_{sol}$ = 25.9 kcal·mol^{-1}.

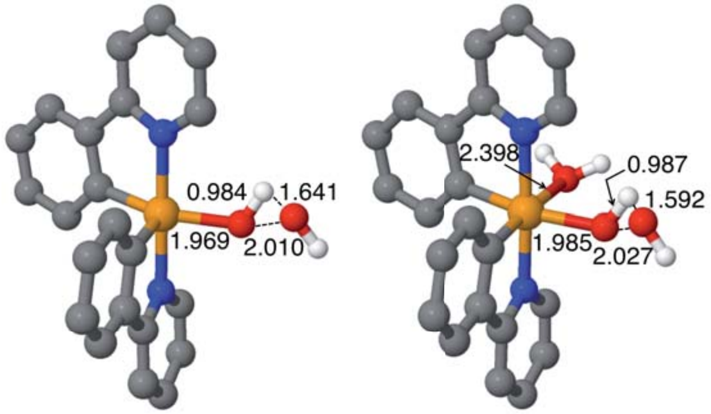

Figure 4.4: Optimized geometries of **O-TS** (left) and **O-TS'** (right). The H atoms of the phpy ligand are removed for clarity. Elements color code: orange = Ir, blue = N, red = O, gray = C, white = H.

The proposed active species in less acidic conditions is the neutral [Ir(O)(OH)(phpy)$_2$] complex, labeled **OOH** (Scheme 4.4). The optimization of this structure maintains the six-coordinated octahedral geometry around the Ir center with the oxo, d(Ir–O)= 1.837 Å, and hydroxo, d(Ir–OH) = 1.992 Å, ligands in *cis*. In this case, the O–O bond formation mechanism can evolve through two distinct pathways (Figures 4.5 and 4.6), since the proton released by water can be transferred to either the oxo or the hydroxo ancillary ligand.

Both pathways start with the formation of the **OOH-1** complex, in which water makes a hydrogen-bond with the oxo and hydroxo ligands, d(H···O) = 2.208 Å and 2.022 Å, respectively. As it is shown in Figure 4.7, **OOH-TS** involves the nucleophilic attack of water to the Ir(V)=O fragment and proton transfer to the same oxo. The ancillary hydroxo ligand does not participate into the process, thus playing a spectator role. The relaxation of the transition state towards the products-side of the reaction leads to the formation of **OOH-2**, in which the hydrogen peroxide molecule is bounded in a η^1-fashion to the Ir center, d(Ir–O) = 2.324 Å.

In contrast, in the energy profile depicted in Figure 4.6, the hydroxo ligand acts as the proton acceptor, giving rise to the octahedral complex **OOH-2'** with aqua and η^1-OOH ligands coordinated to the metal center in *cis*. The bond distances between these ligands and the metal center are d(Ir–OH$_2$) = 2.310 Å and d(Ir–OOH) = 2.149 Å.

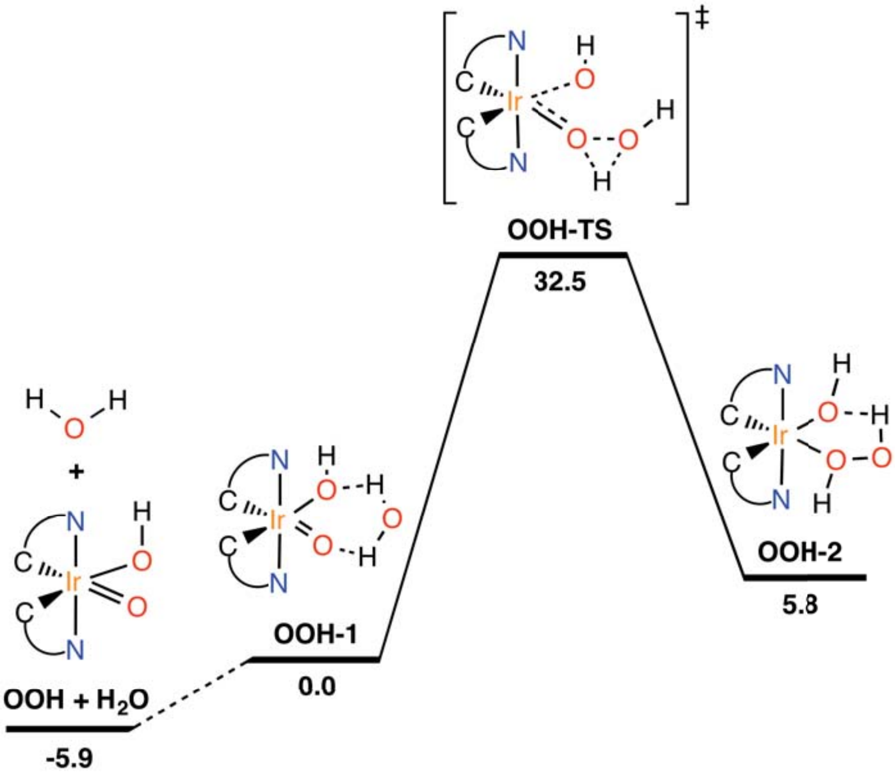

Figure 4.5: Gibbs energy profile, in kcal·mol^{-1}, for the O–O bond formation with the neutral **OOH** active species. The proton acceptor is the oxo ligand. C^N = phpy ligand.

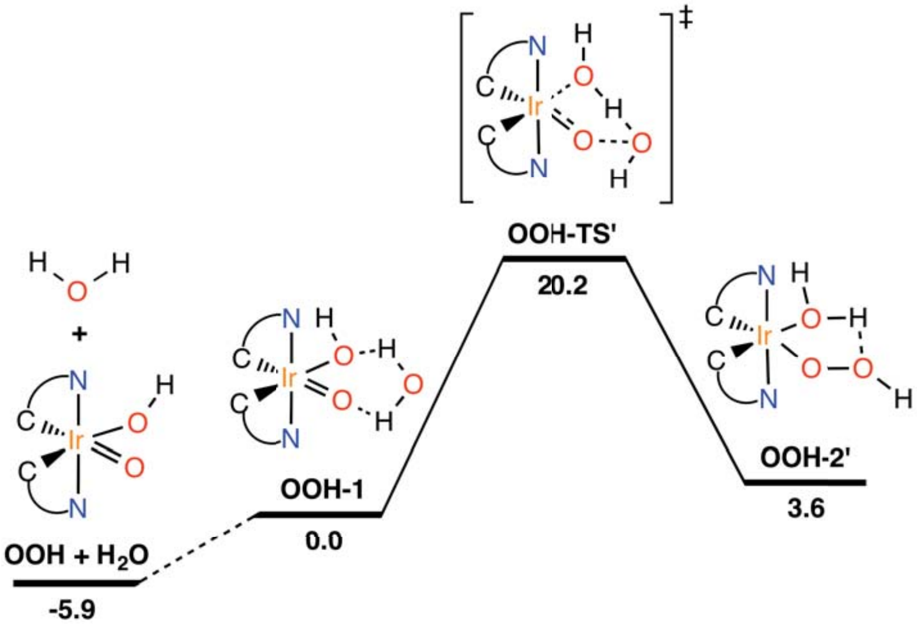

Figure 4.6: Gibbs energy profile, in kcal·mol^{-1}, for the O–O bond formation with the neutral **OOH** active species. The proton acceptor is the hydroxo ancillary ligand. C^N = phpy ligand.

As it can be observed in the Gibbs energy profiles presented in Figures 4.5 and 4.6, when the proton is transferred to the ancillary hydroxo ligand both the transition state and the product become more stable. As consequence, the reaction evolves through a less endoergic pathway, ΔG_{sol} = 3.6 kcal·mol^{-1}, as well as a lower energy barrier, $\Delta G^{\ddagger}_{sol}$ = 20.2 kcal·mol^{-1}.

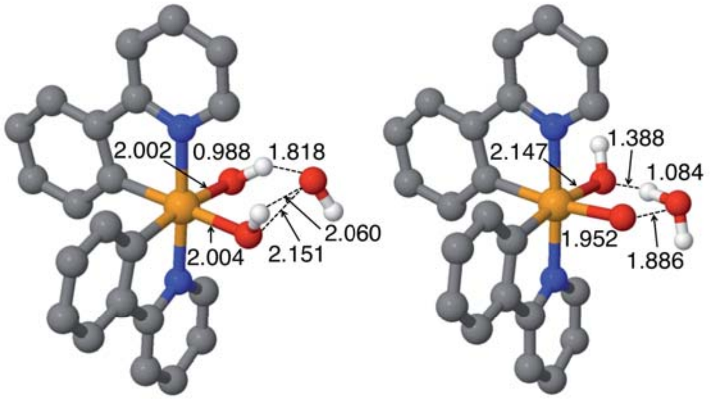

Figure 4.7: Optimized geometries of **OOH-TS** (left) and **OOH-TS'** (right). The H atoms of the phpy ligand are removed for clarity. Elements color code: orange = Ir, blue = N, red = O, gray = C, white = H.

In basic conditions, the active species may be the anionic $[Ir(O)_2(phpy)_2]^-$ complex, labeled **OO** (Scheme 4.4). It has a six-coordinated octahedral structure with both oxo ligands in *cis* position, d(Ir–O) = 1.864 Å.

The reaction of an incoming water molecule with **OO** may follow two distinct reaction pathways. One possibility is that the same oxo ligand accepts the proton and yields the O–O bond, while the other oxo remains unaltered. Unfortunately, this pathway could not be characterized because, despite numerous attempts, we were unable to locate its associated transition state. The other option is that both oxo ligands are involved in the process; one accepting the proton and the other forming the O–O bond (Figure 4.8). This latter pathway was fully characterized and starts with the pre-reaction complex **OO-1** (Figure 4.9), in which water forms a hydrogen-bond with both oxo ligands, d(H···OIr) = 1.984 Å. The reaction evolves through the **OO-TS** transition state, giving rise to the **OO-2** intermediate that contains one hydroxo, d(Ir–OH) = 2.111 Å, and one hydroperoxo ligands, d(Ir–OOH) = 2.146 Å, in *cis*.

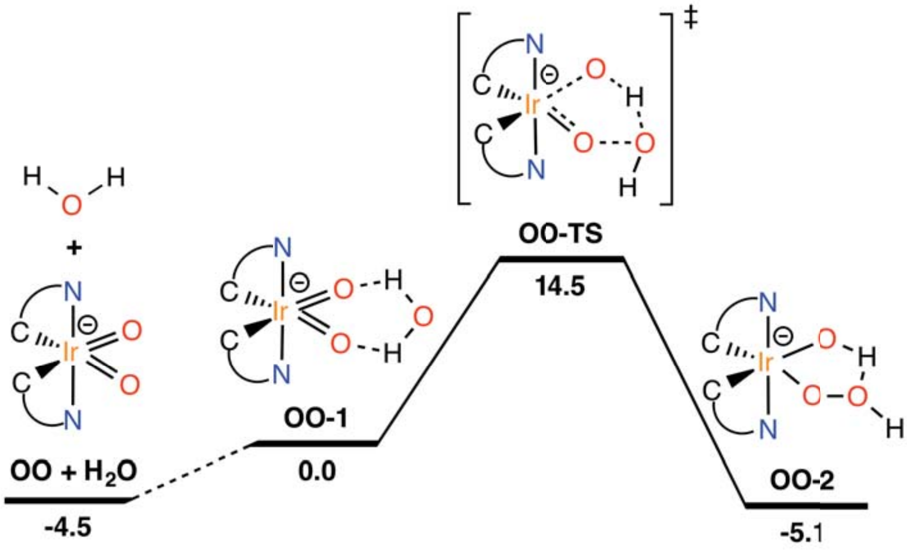

Figure 4.8: Gibbs energy profile, in kcal·mol^{-1}, for the O–O bond formation with the anionic **OO** active species. The proton acceptor is the oxo ancillary ligand.

This reaction path results in the most favorable energy profile among all that have been investigated. It has a moderate energy barrier, $\Delta G^{\ddagger}_{sol}$ = 14.5 kcal·mol^{-1}, and is exoergic by ΔG_{sol} = -5.1 kcal·mol^{-1}.

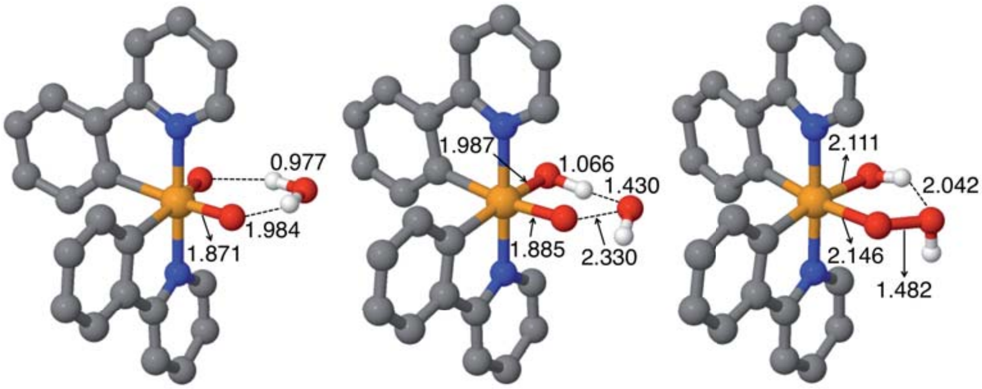

Figure 4.9: Optimized geometry of **OO-1**, **OO-TS** and **OO-2**. The H atoms of the phpy ligand are removed for clarity. Elements color code: orange = Ir, blue = N, red = O, gray = C, white = H.

4.3.2. Electronic Structure Analysis

In order to get further insight into the reactivity of the three different protonation states proposed as active species, their electronic structure was analyzed by means of Natural Population Analysis (NPA) calculations. As has been reported in previous works,[62,217] the ability of these types of systems to promote the formation of the O−O bond with H_2O stems from their different electronic properties. In particular, we focused on the orbitals located on the Ir−O fragment, which include $d_{\pi}(Ir)$-$p_{\pi}(O)$ combinations (Figure 4.10).

In the five-coordinated $[Ir(O)(phpy)_2]^+$ species, the $d_{\pi}(Ir)$-$p_{\pi}(O)$ orbitals correspond to the frontier orbital, i.e. the highest occupied molecular orbital (HOMO) and the lowest unoccupied molecular orbital (LUMO). In particular, the HOMO is the π out-of-phase combination on the IrNN plane, π_N^*, and the LUMO the σ out-of-phase combination on the IrCC plane, σ_C^*. The double occupied HOMO(π_N^*) orbital promotes the reaction by destabilizing the Ir−O bond, while the two-electron vacancy in the LUMO (σ_C^*) favors the nucleophilic attack of water to the Ir(V)=O moiety.[62] Therefore, the hypothetical six-coordinated $[Ir(O)(H_2O)(phpy)_2]^+$ is unstable, since it would entail the occupation of both antibonding orbitals.[227]

Similarly, the $d_{\pi}(Ir)$-$p_{\pi}(O)$ orbitals in the $[Ir(O)(OH)(phpy)_2]$ species are frontier orbitals; both the HOMO and LUMO have indeed π character, π_N^* and π_C^* respectively. Moreover, these are not pure $d_{\pi}(Ir)$-$p_{\pi}(O)$ orbitals located in the Ir(V)=O fragment, since the ancillary ligand OH^- has also some contribution. This reinforces the participation of the OH ligand in the O−O bond formation, by accepting the proton released by water.

Finally, for the anionic complex $[Ir(O)_2(phpy)_2]^-$, the π_N^* also corresponds to the HOMO, whereas π_C^* is ascribed to the LUMO+2 orbital, which lies at a higher energy level. The equal participation of the two oxo ligands in the π_N^* and π_C^* orbitals accounts for the contribution of both of them into the reaction mechanism.

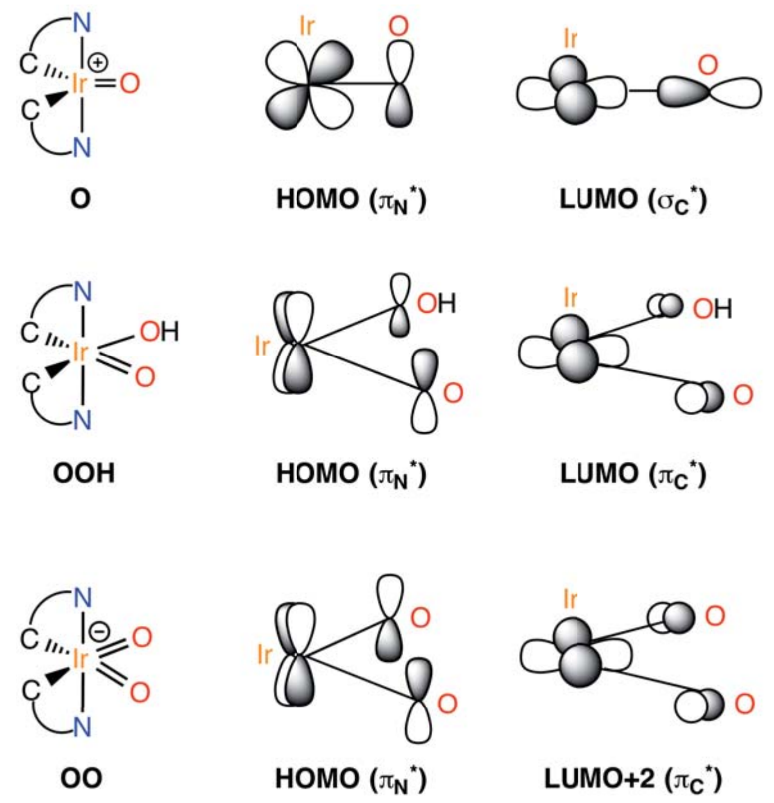

Figure 4.10: Schematic representation of the d_π(Ir)-p_π(O) orbitals.

The energies of the antibonding d_π(Ir)-p_π(O) orbitals for each species, together with the local charges of the Ir(V)=O fragment and X ancillary ligands are given in Table 1.1. As expected, the energy of the HOMO and LUMO orbitals increases when the charge of the active species goes from +1 to -1. Hence, $[Ir(O)_2(phpy)_2]^-$ has the highest HOMO and LUMO, whereas the $[Ir(O)(phpy)_2]^+$ has the lowest ones. Additionally, local charges reflect that $[Ir(O)_2(phpy)_2]^-$ has the most negatively charged X ligand, whereas $[Ir(O)(phpy)_2]^+$ has the most positively charged Ir(V)=O fragment. All these data verify that the cationic species contains the most electrophilic Ir(V)=O moiety, while the anionic one has the most basic ancillary X ligand, O^{2-}. Hence, the intermediate situation corresponds to the neutral $[Ir(O)(OH)(phpy)_2]$ species. The lowest energy barrier found for O−O bond formation with X = O^{2-}, shows the key role played by Brønsted basicity in this reaction.

Table 1.1: Energies of the d_{π}(Ir)-p_{π}(O) orbitals, in hartrees, and the local charges of the Ir=O and X fragments.

Active species	E(HOMO)	E(LUMO)	q(Ir=O)	q(X)
$[Ir(O(phpy)_2]^+$	-0.31351	-0.23160	+0.19	
$[Ir(O)(OH)(phpy)_2]$	-0.17335	-0.07604	+0.02	-0.33
$[Ir(O)_2(phpy)_2]^-$	-0.01416	+0.07903*	-0.17	-0.67

* LUMO+2 orbital

4.4. Discussion and Conclusions

The reactivity of the three protonation states for the Bernhard catalyst was investigated theoretically. The computed energy profiles show that the three $[Ir(O)(X)(phpy)_2]^n$ active species promote the O–O bond formation through an acid/base mechanism, despite of their different degrees of Brønsted basicity and Lewis acidity.

In the cationic system $[Ir(O)(phpy)_2]^+$, the oxo ligand plays a double role by making the O–O bond and taking the proton released by water (Figure 4.2). This pathway involves a high-energy barrier, $\Delta G^{\ddagger}_{sol}$ = 31.9 kcal·mol^{-1}, that stems from the vacant site generated in the metal coordination sphere. This activation barrier is lowered to 25.9 kcal·mol^{-1} by adding an extra water molecule, which assists the process by capping the metal vacant site opened along the reaction pathway (Figure 4.3). On the other hand, in the neutral system, $[Ir(O)(OH)(phpy)_2]$, the proton can be transferred to either the active oxo group (Figure 4.5), $\Delta G^{\ddagger}_{sol}$ = 32.5 kcal·mol^{-1}, or to the ancillary OH^- ligand (Figure 4.6), $\Delta G^{\ddagger}_{sol}$ = 20.2 kcal·mol^{-1}. This decrease in the energy barriers is in accordance with the nature of the corresponding HOMO (π_N^*) orbital.

The lowest energy barrier involves the anionic $[Ir(O)_2(phpy)_2]^-$ species, $\Delta G^{\ddagger}_{sol}$ = 20.2 kcal·mol^{-1}, in which one oxo makes the O–O bond whereas the other accepts the proton lost by the attacking water molecule (Figure 4.8).

Single point calculations at the M06 level yield energy barriers of 31.7, 27.5 and 19.1 kcal·mol^{-1}, for X = OH_2, OH^- and O^{2-}, respectively. It suggests that the activation barriers may be underestimated at the B3LYP level, although the trend followed, in relation with the nature of X, is the same for both functionals.

These results indicate that the Brønsted basicity of the ancillary ligand X has a key influence on the critical O−O bond formation step, even more than the electrophilic character of the Ir(V)=O moiety. In fact, in our catalytic system, the pH media will determine the nature of the ancillary ligand as well as the nature of the reactant, since at basic conditions the O−O bond may be promoted not only by H_2O, but also by the more nucleophilic OH^- anion. In agreement with this, some experiments have shown important pH effects in catalytic water oxidation, when the reaction is driven electrochemically.[44]

Overall, this study provides a way of improving the performance of the water oxidation catalysts. This consists in adding an internal proton acceptor ligand, which remains coordinated to the metal center.[228] These basic ancillary ligands are able to promote the deprotonation of water leading to the much more nucleophilic hydroxide anion that reacts readily with the electrophilic Ir(V)=O moiety to yield the O−O bond. Further, anionic X ligands can stabilize by electron donation the high oxidation states of the metal center, thus reducing the redox potentials required to oxidize the Ir(III) catalyst to the corresponding Ir(V)=O active species. This strategy was proven successful by the cobalt hangman corrole systems of Nocera and co-workers.[229]